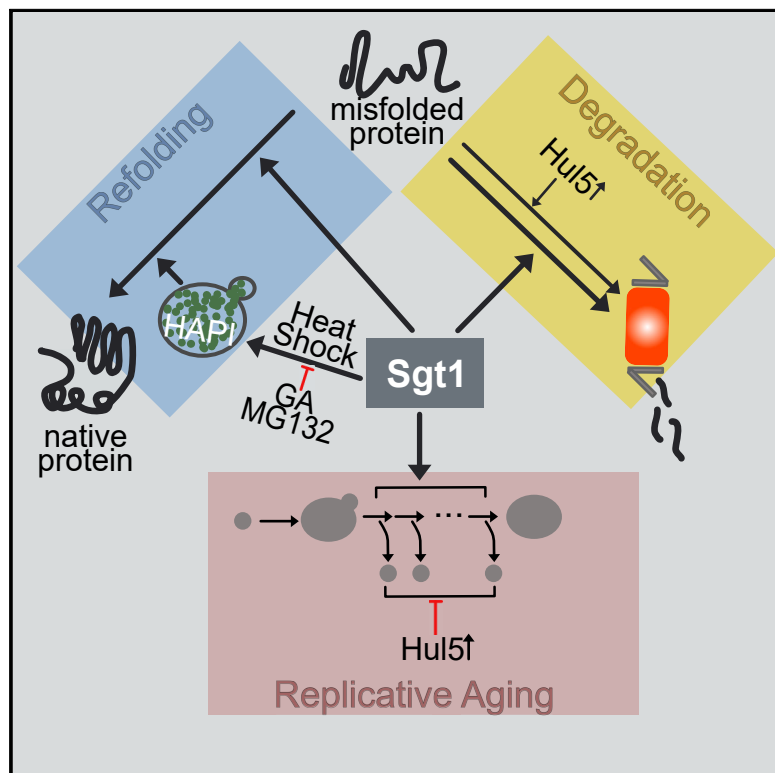


# An Hsp90 co-chaperone links protein folding and degradation and is part of a conserved protein quality control

## Graphical abstract



## Authors

Frederik Eisele,  
Anna Maria Eisele-Bürger, Xinxin Hao,  
Lisa Larsson Berglund, Johanna L. Höög,  
Beidong Liu, Thomas Nyström

## Correspondence

frederik.eisele@gmail.com (F.E.),  
thomas.nystrom@gu.se (T.N.)

## In brief

Eisele et al. demonstrate that the Hsp90 co-chaperone Sgt1 has a widespread role in the folding and degradation of misfolded proteins. Furthermore, Sgt1 localizes upon heat stress to early quality-control sites in an Hsp90- and proteasome-dependent manner, a process that is necessary for efficient resolution of protein inclusions.

## Highlights

- Sgt1 is required for efficient proteasomal degradation of misfolded proteins
- Hul5 partially rescues defects caused by Sgt1 deficiency
- Sgt1 is involved in the merging and subsequent resolution of protein aggregates
- Efficient proteostasis is dependent on Sgt1 and Hsp82 localizing to Q-bodies



## Report

# An Hsp90 co-chaperone links protein folding and degradation and is part of a conserved protein quality control

Frederik Eisele,<sup>1,4,\*</sup> Anna Maria Eisele-Bürger,<sup>1,3,4</sup> Xinxin Hao,<sup>1</sup> Lisa Larsson Berglund,<sup>1,2</sup> Johanna L. Höög,<sup>2</sup> Beidong Liu,<sup>2</sup> and Thomas Nyström<sup>1,5,\*</sup>

<sup>1</sup>Institute for Biomedicine, Sahlgrenska Academy, Centre for Ageing and Health – AgeCap, University of Gothenburg, Medicinargatan 7A, 413 90 Gothenburg, Sweden

<sup>2</sup>Department of Chemistry & Molecular Biology, University of Gothenburg, Medicinargatan 9 C, 413 90 Gothenburg, Sweden

<sup>3</sup>Department of Molecular Sciences, Uppsala BioCenter, Swedish University of Agricultural Sciences and Linnean Center for Plant Biology, PO Box 7015, 75007 Uppsala, Sweden

<sup>4</sup>These authors contributed equally

<sup>5</sup>Lead contact

\*Correspondence: [frederik.eisele@gmail.com](mailto:frederik.eisele@gmail.com) (F.E.), [thomas.nystrom@gu.se](mailto:thomas.nystrom@gu.se) (T.N.)  
<https://doi.org/10.1016/j.celrep.2021.109328>

## SUMMARY

In this paper, we show that the essential Hsp90 co-chaperone Sgt1 is a member of a general protein quality control network that links folding and degradation through its participation in the degradation of misfolded proteins both in the cytosol and the endoplasmic reticulum (ER). Sgt1-dependent protein degradation acts in a parallel pathway to the ubiquitin ligase (E3) and ubiquitin chain elongase (E4), Hul5, and overproduction of Hul5 partly suppresses defects in cells with reduced Sgt1 activity. Upon proteostatic stress, Sgt1 accumulates transiently, in an Hsp90- and proteasome-dependent manner, with quality control sites (Q-bodies) of both yeast and human cells that co-localize with Vps13, a protein that creates organelle contact sites. Misfolding disease proteins, such as synphilin-1 involved in Parkinson's disease, are also sequestered to these compartments and require Sgt1 for their clearance.

## INTRODUCTION

A balanced interplay between the systems involved in protein folding and protein degradation is key for cellular fitness, longevity, and prevention of neurodegenerative diseases. These two processes are often collectively referred to as protein homeostasis or proteostasis (Labbadia and Morimoto, 2015). The folding process is dependent on a network of molecular chaperones (Hartl et al., 2011), whereas the degradation process relies on the ubiquitin proteasome system (UPS) (Amm et al., 2014). A second line of defense in proteostasis, called spatial Protein Quality Control (spatial PQC), sequesters oligomers and aggregated proteins into large inclusions at certain protective locations within the cell (Sontag et al., 2017), a process limiting the toxicity of aberrant proteins. Specifically, upon proteostatic stress of yeast cells, the misfolded proteins initially accumulate at multiple sites, called CytoQs (Miller et al., 2015b), stress foci (Spokoini et al., 2012), or Q-bodies (Escusa-Toret et al., 2013), which later coalesce into larger inclusions at, at least, four distinct spatial quality control sites: the juxtannuclear quality control site (JUNQ); the intranuclear quality control site (INQ); the peripheral, vacuole-associated Insoluble Protein Deposit (IPOD) (Kaganovich et al., 2008; Miller et al., 2015a); and a site adjacent to mitochondria (Braun and Westermann, 2017).

The Hsp90 chaperones represent a major class of chaperones that work together with a variety of co-chaperones (Sahasrabudhe et al., 2017), many of which show high specificity for a small set of client proteins. The Hsp90 co-chaperone Sgt1 (Cattlett and Kaplan, 2006) is known to possess such a specific role as an adaptor protein linking the Skp, Cullin, F-box (SCF) ubiquitin ligase complex to the Hsp90 system and to aid in the assembly of the kinetochore complex (Bansal et al., 2009; Kadota et al., 2010; Kitagawa et al., 1999). Recently, Sgt1 was shown to affect a relatively broad range of client proteins (Sahasrabudhe et al., 2017) indicating a more widespread role in Hsp90 folding processes.

Following two genome-wide screens, we here report that the Sgt1 co-chaperone is a much more general player in cellular PQC than previously anticipated and acts as an important linker, together with Hsp90, between the proteolytic and the folding branches of the proteostatic network.

## RESULTS

### Genome-wide identification of genes required for the degradation of misfolded proteins in the cytosol

To identify components of the PQC system required for the degradation of cytosolic misfolded proteins, we performed a systematic genome-wide screen following the SGA (Synthetic



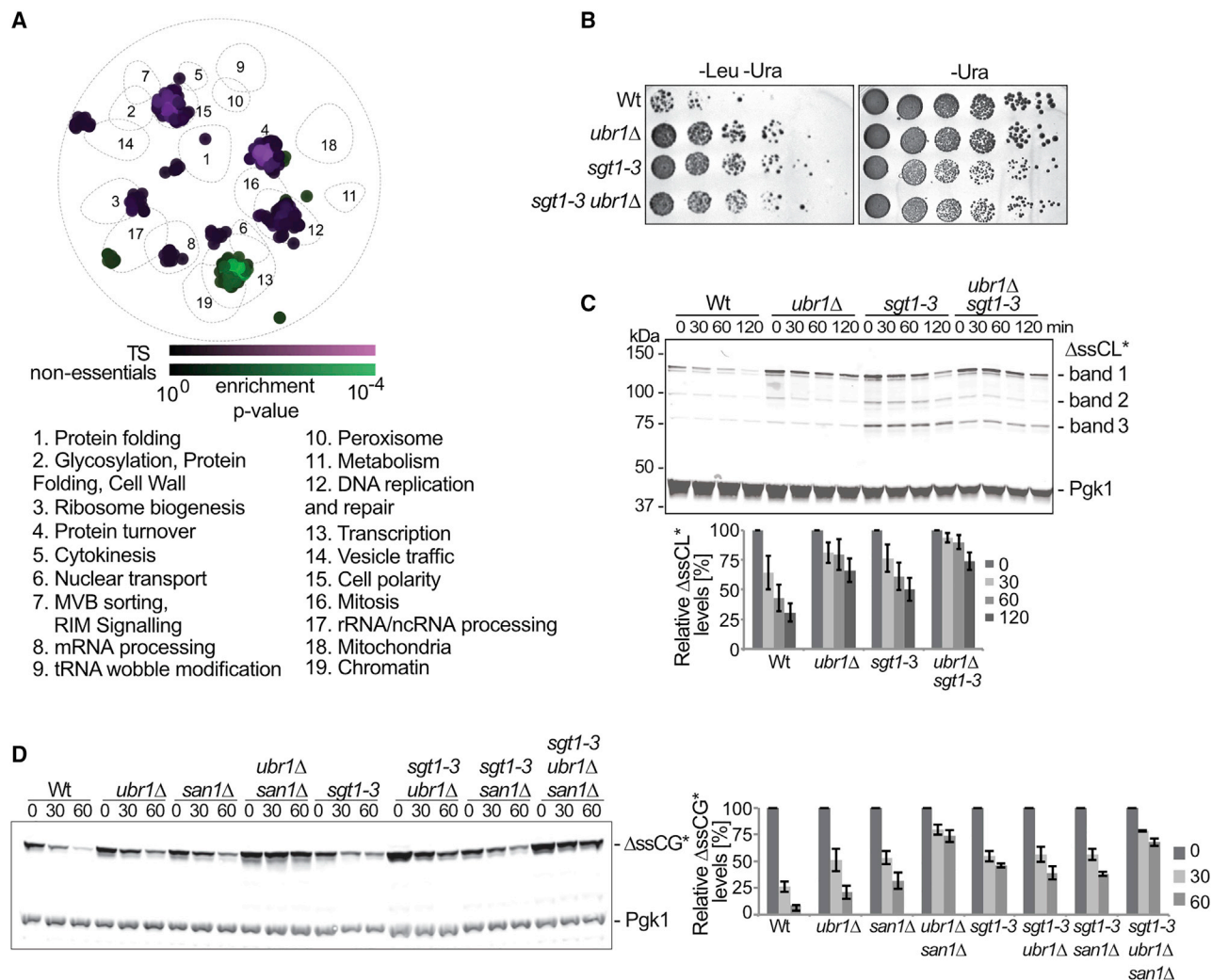


**Figure 1. Identification of the Hsp90 co-chaperone Sgt1 as an essential protein required for the degradation of misfolded cytosolic proteins**

(A) SAFE analysis performed of common hits from two SGA screens of strains expressing one of the chimeric cytosolic substrates,  $\Delta ssCL^*$  or VHL-LEU2, of the 26S proteasome. A cut-off value of  $5e-2$  was chosen for visualization at <https://thecellmap.org>.

(B) Spot test of different strains expressing  $\Delta ssCL^*myc$  on media lacking leucine and uracil (-Leu -Ura) or uracil (-Ura) only as a control.

(C and D) Analysis of  $\Delta ssCL^*$  and  $\Delta ssCG^*$  degradation during a cycloheximide chase at 30°C. Pgk1 served as a loading control. (C) Band 1 indicates full-length and bands 2 and 3 indicate C-terminal partial degradation products of  $\Delta ssCL^*$  detected with antibodies specific for the C-terminal myc tag. (D)  $\Delta ssCG^*$  was detected with antibodies specific for its C-terminal GFP tag. (C and D) Average of three biological replicates was used for quantification. Error bars indicate standard error of the mean (SEM).

See also [Figure S1](#) and [Table S1](#).

Genetic Array) methodology in the complete EUROSCARF deletion library and a collection containing temperature-sensitive (ts) alleles of most essential genes. In both collections, we expressed the misfolding cytosolic mutant of the yeast carboxypeptidase Y ( $\Delta ssCPY^*$ ) fused to Leu2, an often-used prototrophic marker in *Saccharomyces cerevisiae* laboratory strains, tagged with a C-terminal myc tag ( $\Delta ssCL^*$ ). For a second screen, we introduced Von Hippel-Lindau (VHL)-LEU2, encoding the misfolding mammalian VHL tumor suppressor protein (McClellan et al., 2005) fused to Leu2. Due to the misfolding of  $\Delta ssCL^*$  and VHL-Leu2, cells degrade these proteins rapidly (Eisele and Wolf, 2008; McClellan et al., 2005).

Thus, mutants in which the misfolded proteins are stabilized can easily be scored for, because they grow better than wild-type cells on media lacking leucine.

Spatial Analysis of Functional Enrichment (SAFE) (Baryshnikova, 2016; Usaj et al., 2017) of common hits of the two screens showed that four major functional groups among the essential genes were required for proper degradation of the two misfolded proteins. Among the non-essential genes, those linked to the functional groups' transcription, chromatin, and protein turnover were markedly enriched (Figure 1A; Table S1). In contrast, cells with mutations in single genes, essential or non-essential, functioning as chaperones and/or co-chaperones did not display

defects in the degradation of misfolded cytosolic proteins, suggesting that the chaperone/co-chaperone network of the cell is genetically well buffered. However, there was one noteworthy exception: the Hsp90 co-chaperone Sgt1.

Cells with reduced activity of Sgt1 displayed enhanced growth on plates lacking leucine and grew as well as cells lacking the ubiquitin ligase Ubr1, which has previously been shown to be a key factor in tagging misfolded  $\Delta$ ssCPY\* for degradation (Eisele and Wolf, 2008; Heck et al., 2010). Combining the *sgt1-3* mutation with an *UBR1* deletion did not result in additive effects, demonstrating that they act in common pathways (Figure 1B). The *sgt1-3*-dependent stabilization of  $\Delta$ ssCL\* could be complemented by extra-chromosomal *SGT1* expression, and we confirmed that the Hsp90 system and Sgt1 are not involved in the folding or degradation of the Leu2-myc domain alone (Figures S1A and S1B).

*SGT1* mutants displayed an enhanced sensitivity to the proline analog, AZC, which causes severe and general protein misfolding (Trotter et al., 2001) (Figure S1C). The data suggest that Sgt1 might be a more general player in cytosolic quality control than previously anticipated with a functional link to degradation of misfolded cytosolic proteins. Further, we observed that the *sgt1-3 ubr1 $\Delta$*  double mutant showed a reduced heat sensitivity compared with the *sgt1-3* mutant alone (Figure S1D). Ubr1 is known to have a role in degradation of several ts mutants (Khosrow-Khavar et al., 2012), and we could demonstrate that Sgt1 mutant protein also is a substrate of this E3 ligase (Figure S1E).

### The Hsp90 co-chaperone Sgt1 physically interacts with cytosolic misfolded proteins and is required for their degradation

Cycloheximide chase experiments demonstrated that the rate of degradation of  $\Delta$ ssCL\* was delayed in cells with reduced Sgt1 activity to almost the same extent as in cells lacking Ubr1 (Figure 1C). However, degradation of  $\Delta$ ssCL\* was not much altered in a mutant of *CDC34*, the ubiquitin-conjugating enzyme (E2) of the SCF complex, demonstrating a Sgt1 role independent of this complex (Figure S1F). Moreover, Sgt1 and  $\Delta$ ssCL\* interacted physically, indicating a direct role for Sgt1 in modulating the stability of this misfolded substrate (Figure S1G). Degradation of VHL in the *sgt1-3* mutant was also retarded (Figure S1H). Previously, VHL degradation was shown to be dependent on Hsp90s (McClellan et al., 2005); however, cycloheximide chase experiments of  $\Delta$ ssCL\* in the presence of Hsp90 inhibitor geldanamycin (GA) in *hsc82 $\Delta$*  or *sgt1-3* strains did not support a role for Hsp90 in degradation of this substrate (Figure S1I). Also, the physical interaction between Sgt1 and  $\Delta$ ssCL\* was not altered when Hsp90 activity is inhibited, neither by deletion of *Hsc82* nor by addition of GA (Figure S1G).

A GFP-tagged version of misfolded cytosolic CPY\* ( $\Delta$ ssCG\*) has previously been shown to be dependent on both the nuclear localized E3 ligase San1 and the cytoplasmic Ubr1 for its proteasomal degradation (Heck et al., 2010). If one of the two ligases was deleted, degradation of  $\Delta$ ssCG\* was only slightly delayed. However, double deletions of *UBR1* and *SAN1* led to strong stabilization of this substrate (Heck et al., 2010) (Figure 2C). We found that *sgt1-3* mutation stabilized  $\Delta$ ssCG\* more than either one of the single *ubr1 $\Delta$*  and *san1 $\Delta$*  mutations (Figure 1D). Combining *sgt1-3*

with single mutants in *UBR1* or *SAN1* did not result in additive effects, suggesting that Sgt1 is a key co-factor in the Ubr1/San1-dependent degradation of  $\Delta$ ssCG\*. A summary of factors involved in quality control of established fusion model substrates used in this study can be found in Table 1.

### Sgt1 is required for endoplasmic reticulum (ER)-associated degradation (ERAD) in parallel with the multi-ubiquitin chain assembly factor Hul5

We noticed that fragments derived from  $\Delta$ ssCL\* degradation accumulated in *sgt1-3* cells with sizes around 100 and 75 kDa (bands 2 and 3, respectively; Figure 1C). A similar accumulation of fragments of the ERAD substrate CTL\*, a model substrate consisting of the ER luminal ERAD substrate CPY\* fused to a transmembrane domain and Leu2 (Medicherla et al., 2004), has been reported previously in cells lacking Hul5 (Kohlmann et al., 2008), a ubiquitin ligase (E3)/ubiquitin chain elongating enzyme (E4) (Crosas et al., 2006). We found that similar fragments of  $\Delta$ ssCL\* accumulated in *hul5 $\Delta$*  cells (Figures 2A and S2A). Like for CTL\* (Kohlmann et al., 2008), deletion of *HUL5* had no effect on degradation of full-length  $\Delta$ ssCL\*. Deleting *HUL5* in the *sgt1-3* mutant generated an additive effect on the stabilization of fragments, and overproduction of Hul5 in *sgt1-3* cells suppressed such accumulation of fragments (Figures 2A and S2A). The accumulation of  $\Delta$ ssCL\* fragments containing Leu2 in *sgt1-3* and *hul5 $\Delta$*  strains explains their enhanced growth on media lacking leucine (Figure S2B). We discovered more ubiquitylated  $\Delta$ ssCL\* was accumulating in the *sgt1-3* mutant. Overexpression of *HUL5* led to a wild-type-like ubiquitylation state and to suppression of the enhanced ubiquitylation phenotype of the *sgt1-3* strain. A *HUL5* deletion led to comparably lower ubiquitylation levels than the *sgt1-3* mutant. As expected, the *UBR1* deletion strain displayed a markedly reduced ubiquitylation of this substrate (Figure S2C).

Because Hul5 has been shown to be required for the degradation of some ERAD substrates (Kohlmann et al., 2008), we tested if this was true also for Sgt1. Indeed, CTL\* was stabilized in *sgt1-3* cells, and two fragments, corresponding to those accumulating in *hul5 $\Delta$*  cells (Kohlmann et al., 2008), were found to accumulate also in *sgt1-3* cells (bands 2 and 3; Figure 2B). Again, stabilization of CTL\* fragment accumulation and enhanced growth on plates lacking leucine of *sgt1-3* cells could be suppressed by elevating Hul5 levels (Figures 2B and S2D). The ER luminal misfolded ERAD substrate CPY\*-HA (Taxis et al., 2002) was also dependent on proper *SGT1* functionality for its degradation, and *HUL5* overexpression improved the degradation of this substrate in the *sgt1-3* mutant (Figure 2C). In contrast, the previously described cytosolic Hsp70-dependent degradation of the ERAD substrate CTG\* (Taxis et al., 2003) was not dependent on Sgt1 (Figure S2E), ruling out the possibility that mutation in *SGT1* leads to a general inhibition of the 26S proteasome. Taken together, the data suggest that Sgt1 and Hul5 act in parallel pathways and display similar mechanisms involved in protein degradation.

### Overproduction of Hul5 increases the fitness and longevity of cells mutated in SGT1

Mutation in *SGT1* caused severe fitness defects, but overexpression of *HUL5* could partially compensate for reduced Sgt1 activity

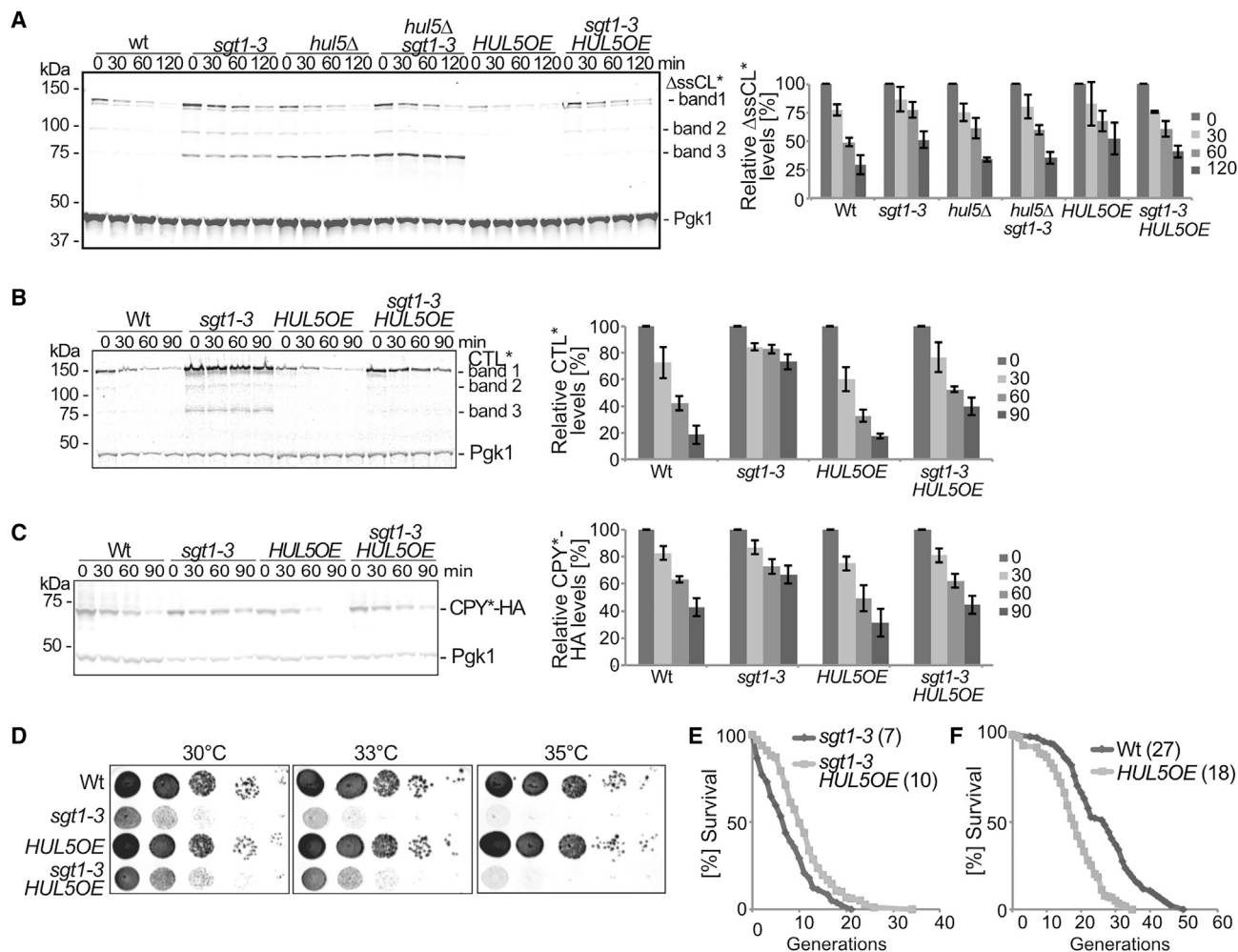


**Figure 2. Reduction in processing of misfolded proteins of the cytoplasm and the ER and of fitness and replicative lifespan caused by *SGT1* deficiency can be partially suppressed by overexpressing *HUL5***

(A–C) Cycloheximide chase analysis of  $\Delta$ ssCL\* (A), CTL\* (B), and CPY\*-HA (C) in indicated strains grown at 30°C. Full-length band 1 of  $\Delta$ ssCL\* and CTL\* detected with anti-myc, CPY\*-HA with anti-HA antibodies. P<sub>gk1</sub> served as a loading control. Bars represent relative average protein levels, and error bars indicate SEM of three biological replicates.

(D) 5-fold dilution series of indicated strains on YPD incubated at indicated temperatures.

(E) Replicative lifespan of *sgt1-3* (n = 96) and *sgt1-3 HUL5* overexpression strain (n = 101; p < 0.0001, log-rank [Mantel-Cox] test).

(F) Replicative lifespan of wild-type (Wt) (n = 102) and *HUL5* overexpression strain (n = 124; p < 0.0001, log-rank [Mantel-Cox] test). Numbers in parentheses indicate the median replicative lifespan of each strain.

See also Figure S2.

up to 33°C (Figure 2D). Similarly, the rate of replicative aging was drastically accelerated in *sgt1-3* cells, and overproduction of Hul5 could retard such aging to a certain degree (Figure 2E). In contrast, Hul5 overproduction alone accelerated replicative aging (Figure 2F). Deletion of *HUL5* had no effect, while overexpression of *SGT1* caused a modest decrease in lifespan (Figure S2F).

#### Sgt1 is required for aggregate coalescence and clearance

Using a GFP-tagged version of the yeast disaggregase Hsp104, which specifically binds to aggregated proteins (Erjavec et al., 2007; Spokoini et al., 2012), we found that a larger fraction of *sgt1-3* cells growing at 30°C contained aggregates compared

with wild-type cells (Figure 3A). Upon heat shock at 38°C for 90 min, *sgt1-3* cells failed to form the typical one to two protein inclusions seen in wild-type cells and instead exhibited multiple (three or more; type 3 cells) aggregates in the cytoplasm (Figures 3A and S3A). Moreover, when cells were incubated at 42°C for 30 min and then allowed to recover at 30°C for 90 min, the rate of clearance of aggregates was markedly delayed in *sgt1-3* cells (Figure S3B). This delay of recovery did not correlate with increased cell death in the *ts sgt1-3* mutant (Figure S3C). The disaggregation of Ubc9ts-GFP, a fusion protein of a *ts* allele of *UBC9* that misfolds upon a 38°C heat shock (Kaganovich et al., 2008), was also delayed in cells with reduced Sgt1 activity (Figures S3D and S3E).

**Table 1. Fusion model substrates used in this study**

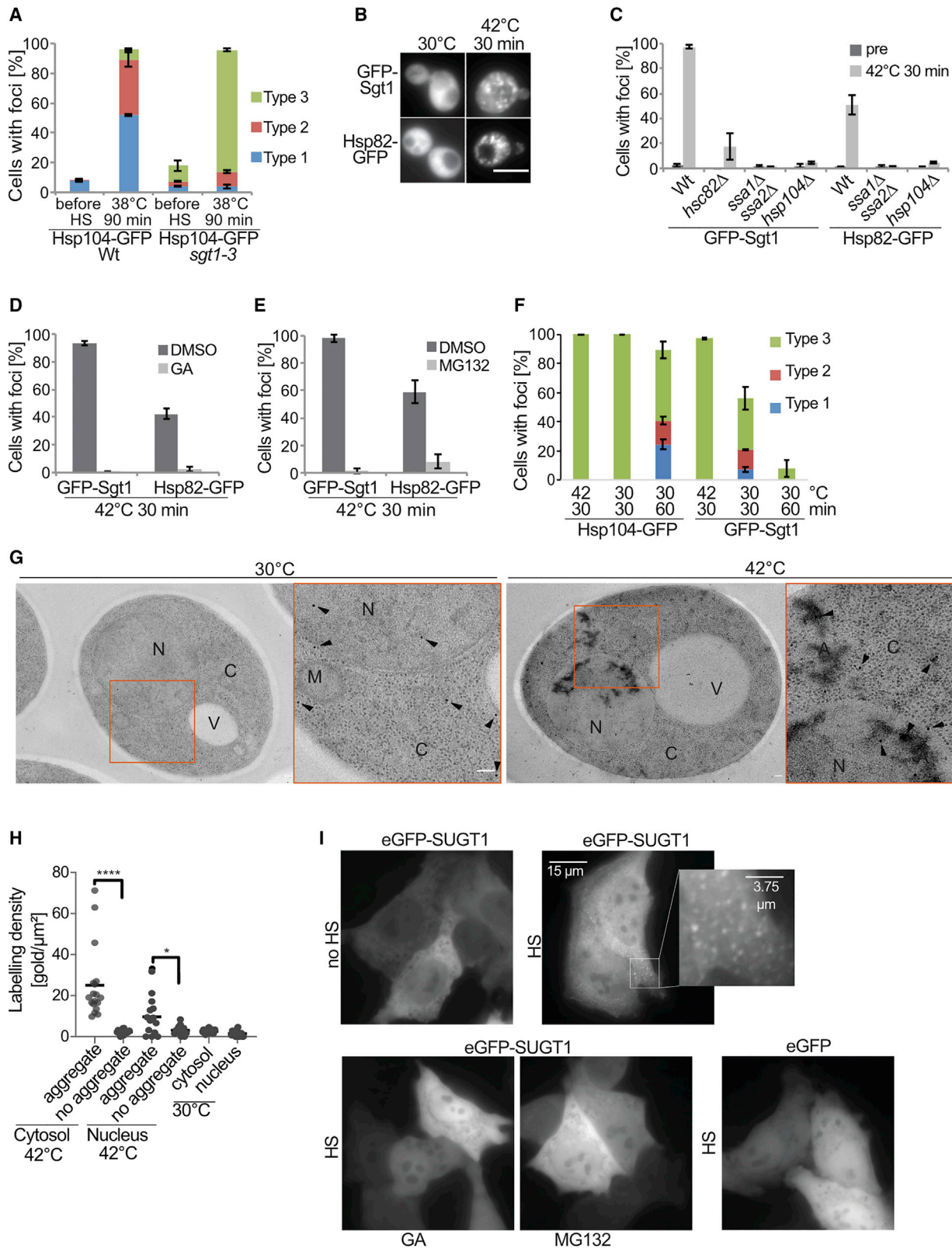
Fusion model substrate proteins	Examples of previously shown factors involved in protein quality control	References
$\Delta$ ssCL*	Ubr1; Ubp3; Ssa1/2/4; Tsa1; Hsp31/32/33	Eisele and Wolf (2008) Öling et al. (2014) Andersson et al. (2021) Hanzén et al. (2016) Amm et al. (2015)
VHL-GFP	Proteasome; Ubc4/5; JUNQ/INQ, IPOD, Sti1; Fes1; Hsp104; Sis1; Btn2; Hsp42	Kaganovich et al. (2008) Malinovska et al. (2012); Ho et al. (2019); Miller et al. (2015a)
$\Delta$ ssCG*	Ssa1, proteasome, Ubc4/5; Ubr1, San1, Ubp3; Tsa1; Ssa1/2/4	Park et al. (2007) Heck et al. (2010) Öling et al. (2014) Hanzén et al. (2016) Andersson et al. (2021)
CTL*	Dsk2, Rad23; Hul5	Medicherla et al. (2004) Kohlmann et al. (2008)
CPY*HA	ER to Golgi factors	Taxis et al. (2002)
CTG*	proteasome, Ubc1/7, Hrd1, Cdc48, Ssa1, Hsp104	Taxis et al. (2003)
Ubc9ts-GFP	proteasome; Ubc4/5, JUNQ, IPOD, Q-bodies, Ubp3, Sis1, Hsp104	Kaganovich et al. (2008) Escusa-Toret et al. (2013) Öling et al. (2014) Malinovska et al. (2012)
dsRed-Synphilin-1	genes involved in cytoskeleton organization, histone modification, sister chromatid segregation, glycolipid biosynthetic process, DNA repair, and replication are required for synphilin-1 inclusion formation	Zhao et al. (2016)
Guk1-7-GFP	Ubr1, proteasome, Gim3, Sed5, Ssa1/2/4	Comyn et al. (2016) Babazadeh et al. (2019) Andersson et al. (2021)

Sgt1 was found to be crucial also for alleviating accumulation of aggregates during aging (Figure S3F). Moreover, although the “middle-aged” (10–15 generations old) wild-type cells displayed mainly one or two inclusions, middle-aged *sgt1-3* cells contained multiple aggregates (Figure S3F).

### Sgt1 clusters in a quality control compartment dependent on Hsp90 and proteasome activity

Spatial quality control sites in yeast include JUNQ, INQ, IPOD, and CytoQs (Escusa-Toret et al., 2013; Kaganovich et al., 2008; Miller et al., 2015a, 2015b; Spokoini et al., 2012). We used a GFP-tagged version of *SGT1* to elucidate if Sgt1 accumulates at any such sites. By crossing GFP-*SGT1* with a *sgt1-3* strain, we found that the *sgt1-3* allele was fully complemented demonstrating the functionality of the tagged GFP-Sgt1 protein (Figure S3G). We found that GFP-Sgt1 normally displayed a uniform distribution in the cytosol and nucleus. However, when cells were subjected to a heat shock at 42°C, the fusion protein formed multiple small foci (Figure 3B). Because Sgt1 is a known co-chaperone of Hsp90s (Hsp82 and

Hsp82), we tested if Hsp82-GFP accumulated in similar foci (Figure 3B) and found overlapping GFP-Sgt1 and Hsp82-Ruby foci (Figure S3H). Deleting the constitutive Hsp90 gene, *HSC82*, drastically reduced formation of the GFP-Sgt1 foci upon heat shock (Figure 3C), and inhibiting Hsp90 activity with GA prevented both Sgt1 and Hsp82 foci formation (Figure 3D). In addition, Sgt1 and Hsp82 foci formation required the Hsp70s Ssa1 and Ssa2 and the disaggregase Hsp104 (Figure 3C), but not the small heat shock protein, Hsp42, which is an essential factor for sequestration of misfolded proteins to peripheral aggregates and Q-bodies (Escusa-Toret et al., 2013; Specht et al., 2011) (Figure S3I). By co-expressing Hsp42-Ruby with GFP-Sgt1, we found that both foci partially overlap after a heat shock at 42°C, but after recovery at 30°C, Sgt1 foci resolve quickly, while Hsp42 foci remain and coalesce into few inclusions free of Sgt1 (Figure S3J). We also found that proteasome activity was required for Sgt1 and Hsp90 foci formation (Figure 3E). Therefore, we refer to these foci as Hsp70/90/104 and proteasome-dependent heat-induced inclusions (HAPIs) that are formed transiently during proteostatic stress and that do



(legend on next page)

not appear to coalesce (Figures 3F and S3K). HAPIs seem to be unstable because they cannot be fixed with formaldehyde, which suggests that they are dynamic complexes that transiently co-localize with Hsp42-containing Q-bodies before such bodies coalesce into IPODs (Figure S3L). No foci were formed after heat shock by Skp1-GFP, the SCF complex backbone protein, suggesting no involvement of this complex in HAPI formation (Figure S3M).

Immunoelectron microscopy of cryofixed GFP-Sgt1 cells grown at 30°C (Figure 3G) showed a rather random distribution of gold particles after labeling of the sectioned cells with GFP-specific and gold-conjugated secondary antibodies (Figure 3G). However, cells that were heat shocked displayed protein aggregation that appears as electron dense clusters in the electron micrographs. We found that gold particles displayed a higher density in these areas of protein aggregation both in the cytosol and the nucleus (Figures 3G and 3H).

Because no transient foci have been described yet for Hsp90s or its co-chaperones, we tested the behavior of GFP-tagged human Sgt1 homolog SUGT1 in HeLa cells. At 37°C, GFP-SUGT1 was evenly distributed in the cytosol but formed HAPI-like-shaped foci when cells were switched to 40°C. Again, cells treated with Hsp90 or proteasome inhibitor were unable to form foci (Figure 3I), demonstrating conservation of this phenomenon.

We performed pull-down experiments of GFP-Sgt1 from yeast cells growing at 30°C and cells heat shocked for 30 min at 42°C, and we used mass spectrometry to identify proteins that bind to GFP-Sgt1 at both 30°C and 42°C. In this group, components of the SCF complex and the Hsp90 machinery were strongly enriched (Table S2). Proteins enriched in binding to GFP-Sgt1 exclusively at 42°C have roles in endosome formation and trafficking, and many are found to be associated with the plasma membrane and nuclear periphery (Table S2; Figure 4A). One protein of this group is the heat-stress-induced Btn2, which plays an important role as a chaperone and sequestrase for misfolding proteins, a triage between refolding and degradation (Ho et al., 2019; Malinowska et al., 2012; Miller et al., 2015a). Also, Vps13 was co-purified with Sgt1 exclusively at 42°C. In human, nonfunctional Vps13 can cause the progressive movement disorder chorea-acantho-

cytosis, the developmental disorder Cohen syndrome, Parkinson's disease, or spastic ataxia (Kolehmainen et al., 2003; Lesage et al., 2016; Rampoldi et al., 2001; Seong et al., 2018). Because Vps13 is concentrated at membrane contact sites, Vps13 foci can already be observed before heat shock in a strain harboring a Vps13-GFP (Lang et al., 2015). These foci increased drastically in number after heat shock at 42°C and co-localized transiently with Hsp82 (Figure 4B). However, different from Hsp82, increased foci formation of Vps13 could also be observed with the Hsp90 inhibitor GA (Figure 4B). During recovery from heat shock, Vps13 foci were rapidly reduced to normal levels. However, under conditions when Hsp82 or Sgt1 was not able to form heat-induced foci, e.g., GA treatment, the clearance of Vps13 foci was markedly retarded (Figure 4C). Similar results were obtained when the clearance of foci following a heat shock was examined using the disaggregase Hsp104 (Figure S4A) and the aggregation-prone protein Guk1-7 (Babazadeh et al., 2019) (Figure S4B).

A protein interacting with Sgt1 at 30°C and 42°C was the Hsp70/Hsp90 co-chaperone Sti1 (Wolfe et al., 2013) (Table S2). With its TPR domain-containing regions, Sti1 and its mammalian ortholog HOP (Hsp70-Hsp90 organizing protein) have been shown to bind to the EEVD motives of Hsp70s and Hsp90s to form a ternary complex (Hernández et al., 2002). No HAPI formation could be observed in strains deleted for *STI1* (Figure S4C), indicating the need for this Hsp70- and Hsp90-linking protein in the recruitment of the Hsp90 machinery to HAPIs.

### The aggregated form of the Parkinson's disease protein, synphilin-1, co-localizes with Sgt1 and requires Sgt1 for its clearance

When the recombinant synphilin-1 protein of Parkinson's disease (Wakabayashi et al., 2000) is expressed in exponentially growing yeast cells, only a small fraction of synphilin-1 forms inclusions (Büttner et al., 2010). Upon shift to 42°C, all synphilin-1 formed foci, which were rapidly cleared when the temperature was lowered to 30°C, and this clearance was again dependent on a functional Hsp90 system (Figure 4D). When co-expressed with GFP-tagged Sgt1, a high number of heat-shocked cells displayed co-localization of synphilin-1 and Sgt1. This

### Figure 3. Sgt1 is required for aggregate coalescence and clearance during stress, and it clusters upon heat stress together with Hsp82 in an Hsp90 and proteasome activity-dependent process to Q-bodies

(A) Exponentially growing cells expressing Hsp104-GFP were shifted from 30°C to 38°C for 90 min. (A and F) Bars display total amount of cells with foci and are divided into three types dependent on the amount of foci per cell (type 1 cells [blue] containing one, type 2 cells [red] containing two, or type 3 cells [green] containing three or more foci).

(B) Representative pictures of exponentially growing GFP-Sgt1- or Hsp82-GFP-expressing cells were shifted from 30°C to 42°C for 30 min and analyzed by fluorescence microscopy for foci formation. Scale bar indicates 5 μm.

(C) Percentage of cells forming GFP-Sgt1 or Hsp82-GFP foci in indicated strains before and after heat shock.

(D and E) GFP-Sgt1 or Hsp82-GFP foci formation upon inhibition of Hsp90 activity by adding 70 μM geldanamycin (GA) (D) and proteasome inhibition using 150 μM MG132 when shifted to 42°C (E). DMSO served as a solvent of both drugs and as a negative control.

(F) Clearance of heat shock-induced (42°C for 30 min) Hsp104-GFP and GFP-Sgt1 foci after 30 and 60 min recovery at 30°C. Bars are described under (A).

(G) Thin sections of GFP-Sgt1-expressing yeast cells grown at 30°C or shifted to 42°C for 30 min. Sections were immunogold labeled for visualization of Sgt1 localization. Gold particles are marked with arrowheads. A, electron-dense regions representing protein aggregates; C, cytosol; M, mitochondria, N, nucleus; V, vacuole. Scale bars indicate 100 nm.

(H) Sgt1 localization (gold labeling density) inside and outside of cytosolic and nuclear protein aggregates (electron-dense clusters) were assessed at 30°C (n = 20 cells) and 42°C (n = 19 cells). Wilcoxon matched-pairs signed rank test, \*\*\*\*p < 0.0001, \*p = 0.0105.

(I) Foci formation of human Sgt1 (EGFP-SUGT1) in HeLa cells. Cells were shifted to 40°C and mock treated (DMSO), or GA or MG132 treated. Inset shows a zoom for better visualization of EGFP-SUGT1 foci. EGFP-SUGT1-expressing cells grown at 37°C (no HS) or EGFP after 30 min heat shock at 40°C are shown as negative controls.

All data presented in the bar graphs are an average of n ≥ 3 biological replicates ± SEM. See also Figure S3.

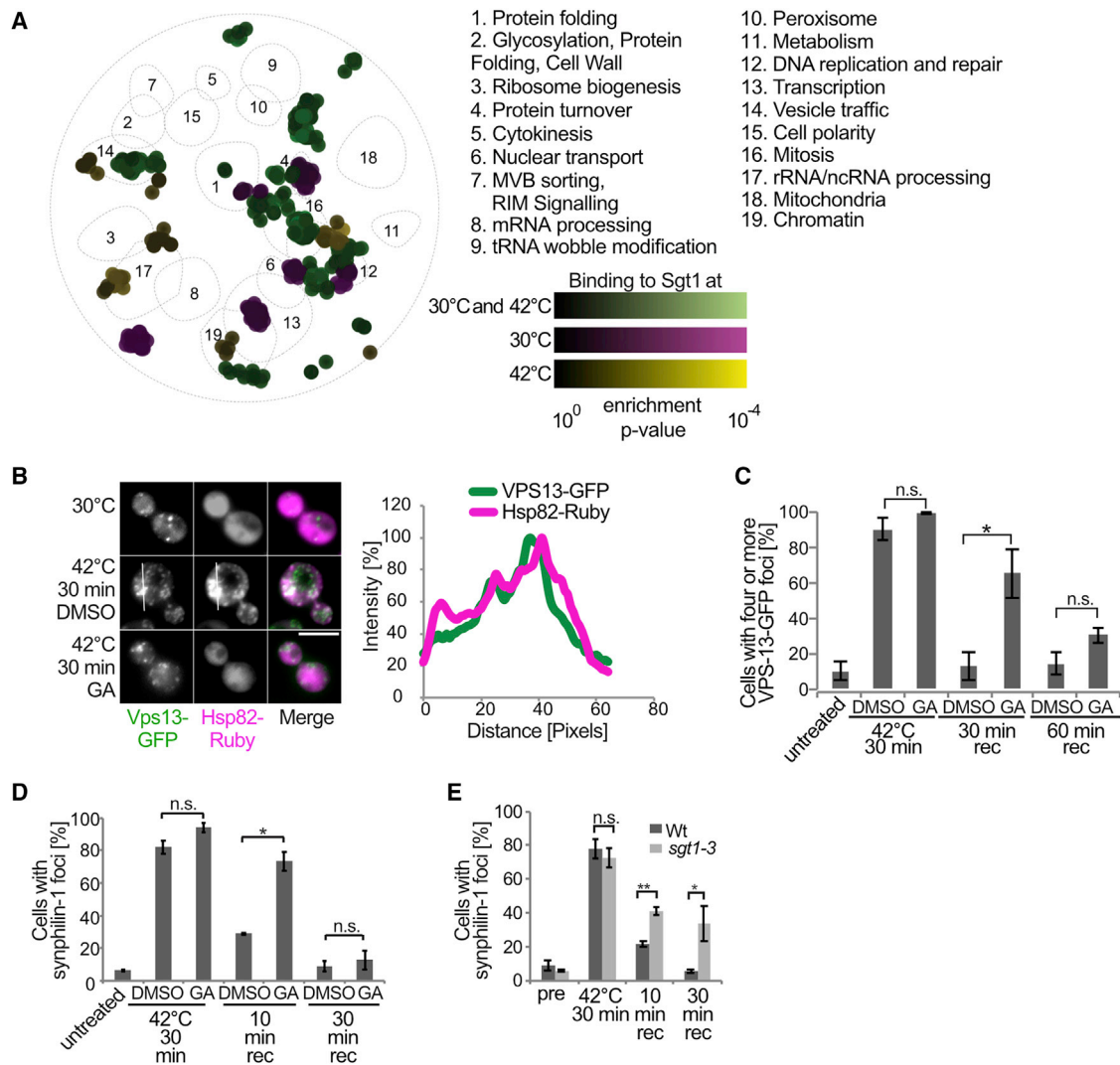


**Figure 4. Physical interactors of Sgt1 at 30°C and 42°C and how their properties are influenced by HAPI formation**

(A) Mass spectrometry analysis of GFP-Sgt1 co-purifying proteins from cells grown at 30°C or heat shocked at 42°C for 30 min ( $n = 4$  biological replicates). SAFE analysis of hits from the screen that bind at 30°C and 42°C (green), exclusively at 30°C (purple) and at 42°C (yellow). A cut-off value of  $5e-2$  was chosen for visualization at <https://thecellmap.org>.

(B) Vps13-GFP foci partially overlap with Hsp82-Ruby foci when allowed to be formed (DMSO). Line intensity plot of Vps13-GFP and Hsp82-Ruby shows the distribution of relative fluorescence after heat shock across the white line. Scale bar indicates 5  $\mu\text{m}$ .

(C and D) Percentage of four or more Vps13-GFP foci-containing cells (C) or synphilin-1 foci-forming cells (D) was analyzed at 42°C and recovery at 30°C for indicated time points in conditions that allow HAPI formation (DMSO) compared with conditions that do not allow HAPI formation (GA).

(E) Percentage of cells showing synphilin-1 foci in Wt and *sgt1-3* mutant cells was analyzed at 42°C and recovery at 30°C. All data in the bar graphs presented are an average of  $n \geq 3$  biological replicates  $\pm$  SEM. \* $p < 0.05$ , \*\* $p < 0.005$ , unpaired two-tailed t test.

See also [Figure S4](#) and [Table S2](#).

co-localization rapidly disappeared upon return to 30°C ([Figure S4D](#)). In *sgt1-3* cells, resolution of synphilin-1 foci was markedly retarded ([Figure 4E](#)), suggesting that Sgt1 needs to be fully functional to ensure rapid clearance of these inclusions.

## DISCUSSION

The Hsp90s make up 1%–2% of total cellular protein and increase to 4%–6% in stressed cells ([Prodromou, 2016](#)), but their

exact role in handling misfolded proteins and aggregates remains obscure. Although degradation of VHL was shown to be delayed in Hsp90 mutant cells ([McClellan et al., 2005](#)), degradation of variants of the misfolding cytosolic model substrate  $\Delta\text{ssCPY}^*$  was shown to be independent of Hsp90s ([Park et al., 2007](#)). Here we show that the Hsp90 co-chaperone Sgt1 is required for degradation and together with Hsp90s is necessary for aggregate removal of misfolded proteins. Moreover, we found that Hsp90 and Sgt1 are recruited to a transient site early

during heat shock, which appears to be distinct from Q-bodies and IPODs. The peculiarity of HAPI entails the requirement for both proteasome and Hsp70/90/104 activity for HAPI to form (Figures 3C–3E). In contrast, Q-bodies and IPODs appear in higher number and are more persistent in cells with reduced Hsp90 activity and upon inhibition of the 26S proteasome (Escusa-Toret et al., 2013). The foci formed by Sgt1 and Hsp82 are transient; when cells are switched back to 30°C, almost all HAPI are rapidly cleared, while Hsp104-associated foci persist longer (Figure 3F), undergo coalescence into IPODs, and cannot be inhibited by addition of GA (Figure S4A). The observation that HAPI cannot be visualized when cells are fixed after heat shock substantiates its different physical properties (Figure S3L). Previously, an Hsp82-GFP fusion has been used as a marker for Q-bodies formed after heat shock (Saarikangas and Barral, 2015), which raises the question of whether the foci analyzed were Q-bodies, HAPIs, or both. We believe that they may have been both because we found that Sgt1 foci co-localize, like Q-bodies, with all the reporters of aggregates used, and using EM we found that Sgt1 was always associated with aggregates in the cytosol (and nucleus) early during a heat shock. Thus, we propose that HAPIs are transiently associated with Q-bodies during heat stress but, in contrast with Q-bodies, require full Hsp90 and proteasome activity to form. That HAPIs, but not Q-bodies, are formed in Hsp42 mutants indicates that these two subcellular complexes are formed independently before their association.

The role of Sgt1 in aggregate clearance appears mechanistically linked to its role in the degradation of misfolded proteins, and reduced Sgt1 activity results in a drastically impaired proteasomal degradation of misfolded proteins. This process can be partially rescued by overexpression of the proteasome-bound E3/E4 ubiquitin ligase Hul5, which was shown previously to increase the processivity of the proteasome (Crosas et al., 2006; Kuo and Goldberg, 2017). Partial degradation products of the substrates  $\Delta$ ssCL\* and CTL\* accumulate in *sgt1-3* cells just like in *hul5* $\Delta$  cells (Figures 2A and 2B), and even though the misfolding protein  $\Delta$ ssCL\* becomes highly ubiquitylated in the *sgt1-3* mutant, its degradation is markedly inhibited. This indicates that proper Sgt1 function is needed also for the transfer of substrates to the 26S proteasome. *HUL5* overexpression can rescue this accrual of ubiquitylated substrates, probably by its own ubiquitylation activity (Figure S2C). With reduced activity of Sgt1, Hsp90-dependent protein folding cycles are most likely slowed down, but substrates that are already marked with ubiquitin may become further ubiquitylated by Hul5 activity (Fang et al., 2011), which causes transfer from the folding machinery to degradation by the proteasome. Interestingly, aggregate formation is drastically increased in mutants of *SGT1* during replicative aging, and the replicative lifespan of *SGT1* mutant cells is reduced. Overexpression of *HUL5* partly counteracted accelerated aging in Sgt1-deficient cells, indicating that an interplay between the Hsp90/Sgt1 and Hul5 systems is important for longevity assurance.

The role of the Hsp90 co-chaperone Sgt1 in aggregate management and protein degradation is interesting in view of data linking Hsp90 activity to neurodegenerative diseases. Several studies have proposed that Hsp90s stabilize aberrant

disease-associated proteins, and that inhibition of these chaperones could redirect neuronal aggregated proteins for degradation (Luo et al., 2010). Other studies have demonstrated that the Hsp90 co-chaperones, CyP40 and PP5, reduce tau pathology but are repressed in aged and Alzheimer disease patients (Shelton et al., 2017). Interestingly, human Sgt1 concentrations have been shown to be drastically reduced in the brains of Alzheimer disease patients (Spiechowicz et al., 2006). In contrast, a recent study showed that Sgt1 increases in the brain of Parkinson's disease patients (Bohush et al., 2019). The impact of such an increase or decrease is not known, but we show here that aggregates of the Parkinson's disease protein, synphilin-1, co-localize with Sgt1 in HAPIs, and that Sgt1 deficiency and conditions that prevent HAPI formation retard clearance of synphilin-1 aggregates. Based on these observations, we believe the role of Hsp90s, Sgt1, and HAPI formation deserves future attention in the field of neurodegeneration and PQC.

## STAR★METHODS

Detailed methods are provided in the online version of this paper and include the following:

- KEY RESOURCES TABLE
- RESOURCE AVAILABILITY
  - Lead contact
  - Materials availability
  - Data and code availability
- EXPERIMENTAL MODEL AND SUBJECT DETAILS
  - Yeast strains
  - Mammalian cell culture
- METHOD DETAILS
  - Plasmid constructions
  - Genome-wide screen for stabilizers of two misfolding proteins
  - Spot tests
  - Co-immuno purifications (Co-IP)
  - *In vivo* ubiquitination assay
  - Cycloheximide chase
  - Metabolic chase
  - Western blotting
  - Replicative lifespan assay
  - Isolation of old mother cells
  - Assessment of colony forming units (CFU)
  - Hsp104, Hsp42 and Guk1-7 protein aggregation induction
  - Sgt1, Hsp82, Vps13, Hsp42-, and synphilin-1 foci formation assay
  - Cell culture and transient transfection
  - Electron microscopy
  - Mass spectrometry
- QUANTIFICATION AND STATISTICAL ANALYSIS

## SUPPLEMENTAL INFORMATION

Supplemental information can be found online at <https://doi.org/10.1016/j.celrep.2021.109328>.

## ACKNOWLEDGMENTS

We thank the EMBL Proteomics Core Facility in Heidelberg, and in particular Mandy Rettel and Frank Stein for support with mass spectrometry and data analysis. We thank Dieter Wolf, Joris Winderickx, Per Widlund, Rebecca Andersson, and Charlie Boone for kindly sharing yeast strains and plasmids. This work was supported by grants from the Swedish Natural Research Council (VR), the Knut and Alice Wallenberg Foundation (KAW; Wallenberg Scholar), and ERC (Advanced Grant; QualiAge) (to T.N.); by grants from the Swedish Cancer Society (CAN 2012/601, CAN 2015/406, and CAN 2017/643 to B.L.); and by grants from the Swedish Natural Research Council (VR 2011-5923 and VR 2015-04984 to B.L.). We thank Peter Bozhkov for supporting A.M.E.-B. during the revision process by KAW grant (DNR KAW 2018.0026).

## AUTHOR CONTRIBUTIONS

F.E., A.M.E.-B., and T.N. conceived experiments and wrote the manuscript. F.E., A.M.E.-B., X.H., and L.L.B. performed experiments, A.M.E.-B. performed experiments during revision. J.L.H. and B.L. provided expertise and feedback.

## DECLARATION OF INTERESTS

F.E. is now an AstraZeneca employee.

Received: June 8, 2020

Revised: November 30, 2020

Accepted: June 9, 2021

Published: June 29, 2021

## REFERENCES

Amberg, D.C., Burke, D.J., Burke, D., Strathern, J.N., and Laboratory, C.S.H. (2005). *Methods in Yeast Genetics: A Cold Spring Harbor Laboratory Course Manual* (Cold Spring Harbor Laboratory Press).

Amm, I., Sommer, T., and Wolf, D.H. (2014). Protein quality control and elimination of protein waste: the role of the ubiquitin-proteasome system. *Biochim. Biophys. Acta* 1843, 182–196.

Amm, I., Norell, D., and Wolf, D.H. (2015). Absence of the yeast Hsp31 chaperones of the DJ-1 superfamily perturbs cytoplasmic protein quality control in late growth phase. *PLoS ONE* 10, e0140363.

Andersson, R., Eisele-Bürger, A.M., Hanzén, S., Vielfort, K., Öling, D., Eisele, F., Johansson, G., Gustafsson, T., Kvint, K., and Nyström, T. (2021). Differential role of cytosolic Hsp70s in longevity assurance and protein quality control. *PLoS Genet.* 17, e1008951.

Babazadeh, R., Ahmadpour, D., Jia, S., Hao, X., Widlund, P., Schneider, K., Eisele, F., Edo, L.D., Smits, G.J., Liu, B., and Nyström, T. (2019). Syntaxin 5 Is Required for the Formation and Clearance of Protein Inclusions during Proteostatic Stress. *Cell Rep.* 28, 2096–2110.e8.

Bansal, P.K., Nourse, A., Abdulle, R., and Kitagawa, K. (2009). Sgt1 dimerization is required for yeast kinetochore assembly. *J. Biol. Chem.* 284, 3586–3592.

Baryshnikova, A. (2016). Systematic Functional Annotation and Visualization of Biological Networks. *Cell Syst.* 2, 412–421.

Bohush, A., Niewiadomska, G., Weis, S., and Filipek, A. (2019). HSP90 and its novel co-chaperones, SGT1 and CHP-1, in brain of patients with Parkinson's disease and dementia with lewy bodies. *J. Parkinsons Dis.* 9, 97–107.

Brachmann, C.B., Davies, A., Cost, G.J., Caputo, E., Li, J., Hieter, P., and Boeke, J.D. (1998). Designer deletion strains derived from *Saccharomyces cerevisiae* S288C: a useful set of strains and plasmids for PCR-mediated gene disruption and other applications. *Yeast* 14, 115–132.

Braun, R.J., and Westermann, B. (2017). With the Help of MOM: Mitochondrial Contributions to Cellular Quality Control. *Trends Cell Biol.* 27, 441–452.

Büttner, S., Delay, C., Franssens, V., Bammens, T., Ruli, D., Zaunschirm, S., de Oliveira, R.M., Outeiro, T.F., Madeo, F., Buée, L., et al. (2010). Synphilin-1 en-

hances  $\alpha$ -synuclein aggregation in yeast and contributes to cellular stress and cell death in a Sir2-dependent manner. *PLoS ONE* 5, e13700.

Catlett, M.G., and Kaplan, K.B. (2006). Sgt1p is a unique co-chaperone that acts as a client adaptor to link Hsp90 to Skp1p. *J. Biol. Chem.* 281, 33739–33748.

Comyn, S.A., Young, B.P., Loewen, C.J., and Mayor, T. (2016). Prefoldin Promotes Proteasomal Degradation of Cytosolic Proteins with Missense Mutations by Maintaining Substrate Solubility. *PLoS Genet.* 12, e1006184.

Costanzo, M., Baryshnikova, A., Bellay, J., Kim, Y., Spear, E.D., Sevier, C.S., Ding, H., Koh, J.L.Y., Toufighi, K., Mostafavi, S., et al. (2010). The genetic landscape of a cell. *Science* 327, 425–431.

Crosas, B., Hanna, J., Kirkpatrick, D.S., Zhang, D.P., Tone, Y., Hathaway, N.A., Buecker, C., Leggett, D.S., Schmidt, M., King, R.W., et al. (2006). Ubiquitin chains are remodeled at the proteasome by opposing ubiquitin ligase and deubiquitinating activities. *Cell* 127, 1401–1413.

Eisele, F., and Wolf, D.H. (2008). Degradation of misfolded protein in the cytoplasm is mediated by the ubiquitin ligase Ubr1. *FEBS Lett.* 582, 4143–4146.

Erjavec, N., Larsson, L., Grantham, J., and Nyström, T. (2007). Accelerated aging and failure to segregate damaged proteins in Sir2 mutants can be suppressed by overproducing the protein aggregation-remodeling factor Hsp104p. *Genes Dev.* 21, 2410–2421.

Escusa-Toret, S., Vonk, W.I.M., and Frydman, J. (2013). Spatial sequestration of misfolded proteins by a dynamic chaperone pathway enhances cellular fitness during stress. *Nat. Cell Biol.* 15, 1231–1243.

Fang, N.N., Ng, A.H.M., Measday, V., and Mayor, T. (2011). Hsp70 HECT ubiquitin ligase plays a major role in the ubiquitylation and turnover of cytosolic misfolded proteins. *Nat. Cell Biol.* 13, 1344–1352.

Franken, H., Mathieson, T., Childs, D., Sweetman, G.M.A., Werner, T., Tögel, I., Doce, C., Gade, S., Bantscheff, M., Drewes, G., et al. (2015). Thermal proteome profiling for unbiased identification of direct and indirect drug targets using multiplexed quantitative mass spectrometry. *Nat. Protoc.* 10, 1567–1593.

Gatto, L., and Lilley, K.S. (2012). MSnbase—an R/Bioconductor package for isobaric tagged mass spectrometry data visualization, processing and quantitation. *Bioinformatics* 28, 288–289.

Geng, F., and Tansey, W.P. (2008). Polyubiquitylation of histone H2B. *Mol. Biol. Cell* 19, 3616–3624.

Hanzén, S., Vielfort, K., Yang, J., Roger, F., Andersson, V., Zamarbide-Forés, S., Andersson, R., Malm, L., Palais, G., Biteau, B., et al. (2016). Lifespan Control by Redox-Dependent Recruitment of Chaperones to Misfolded Proteins. *Cell* 166, 140–151.

Hartl, F.U., Bracher, A., and Hayer-Hartl, M. (2011). Molecular chaperones in protein folding and proteostasis. *Nature* 475, 324–332.

Heck, J.W., Cheung, S.K., and Hampton, R.Y. (2010). Cytoplasmic protein quality control degradation mediated by parallel actions of the E3 ubiquitin ligases Ubr1 and San1. *Proc. Natl. Acad. Sci. USA* 107, 1106–1111.

Hernández, M.P., Sullivan, W.P., and Toft, D.O. (2002). The assembly and intermolecular properties of the hsp70-Hop-hsp90 molecular chaperone complex. *J. Biol. Chem.* 277, 38294–38304.

Hill, S.M., Hao, X., Grönvall, J., Spikings-Nordby, S., Widlund, P.O., Amen, T., Jörhov, A., Josefson, R., Kaganovich, D., Liu, B., and Nyström, T. (2016). Asymmetric Inheritance of Aggregated Proteins and Age Reset in Yeast Are Regulated by Vac17-Dependent Vacuolar Functions. *Cell Rep.* 16, 826–838.

Ho, C.H., Magtanong, L., Barker, S.L., Gresham, D., Nishimura, S., Natarajan, P., Koh, J.L.Y., Porter, J., Gray, C.A., Andersen, R.J., et al. (2009). A molecular barcoded yeast ORF library enables mode-of-action analysis of bioactive compounds. *Nat. Biotechnol.* 27, 369–377.

Ho, C.T., Grousl, T., Shatz, O., Jawed, A., Ruger-Herreros, C., Semmelink, M., Zahn, R., Richter, K., Bukau, B., and Mogk, A. (2019). Cellular sequestrases maintain basal Hsp70 capacity ensuring balanced proteostasis. *Nat. Commun.* 10, 4851.

- Höög, J.L., Lacomble, S., O'Toole, E.T., Hoenger, A., McIntosh, J.R., and Gull, K. (2014). Modes of flagellar assembly in *Chlamydomonas reinhardtii* and *Trypanosoma brucei*. *eLife* *3*, e01479.
- Huber, W., von Heydebreck, A., Sülthmann, H., Poustka, A., and Vingron, M. (2002). Variance stabilization applied to microarray data calibration and to the quantification of differential expression. *Bioinformatics* *18* (Suppl 1), S96–S104.
- Hughes, C.S., Foehr, S., Garfield, D.A., Furlong, E.E., Steinmetz, L.M., and Krijgsveld, J. (2014). Ultrasensitive proteome analysis using paramagnetic bead technology. *Mol. Syst. Biol.* *10*, 757.
- Hwang, C.-S., Shemorry, A., and Varshavsky, A. (2009). Two proteolytic pathways regulate DNA repair by cotargeting the Mgt1 alkyguanine transferase. *Proc. Natl. Acad. Sci. USA* *106*, 2142–2147.
- Janke, C., Magiera, M.M., Rathfelder, N., Taxis, C., Reber, S., Maekawa, H., Moreno-Borchart, A., Doenges, G., Schwob, E., Schiebel, E., and Knop, M. (2004). A versatile toolbox for PCR-based tagging of yeast genes: new fluorescent proteins, more markers and promoter substitution cassettes. *Yeast* *21*, 947–962.
- Kadota, Y., Shirasu, K., and Guerois, R. (2010). NLR sensors meet at the SGT1-HSP90 crossroad. *Trends Biochem. Sci.* *35*, 199–207.
- Kaganovich, D., Kopito, R., and Frydman, J. (2008). Misfolded proteins partition between two distinct quality control compartments. *Nature* *454*, 1088–1095.
- Khosrow-Khavar, F., Fang, N.N., Ng, A.H.M., Winget, J.M., Comyn, S.A., and Mayor, T. (2012). The yeast *ubr1* ubiquitin ligase participates in a prominent pathway that targets cytosolic thermosensitive mutants for degradation. *G3* (Bethesda) *2*, 619–628.
- Kitagawa, K., Skowrya, D., Elledge, S.J., Harper, J.W.W., and Hieter, P. (1999). SGT1 encodes an essential component of the yeast kinetochore assembly pathway and a novel subunit of the SCF ubiquitin ligase complex. *Mol. Cell* *4*, 21–33.
- Kohlmann, S., Schäfer, A., and Wolf, D.H. (2008). Ubiquitin ligase Hul5 is required for fragment-specific substrate degradation in endoplasmic reticulum-associated degradation. *J. Biol. Chem.* *283*, 16374–16383.
- Kolehmainen, J., Black, G.C.M., Saarinen, A., Chandler, K., Clayton-Smith, J., Träskelin, A.L., Perveen, R., Kiviti-Kallio, S., Norio, R., Warburg, M., et al. (2003). Cohen syndrome is caused by mutations in a novel gene, *COH1*, encoding a transmembrane protein with a presumed role in vesicle-mediated sorting and intracellular protein transport. *Am. J. Hum. Genet.* *72*, 1359–1369.
- Kuo, C.-L., and Goldberg, A.L. (2017). Ubiquitinated proteins promote the association of proteasomes with the deubiquitinating enzyme Usp14 and the ubiquitin ligase Ube3c. *Proc. Natl. Acad. Sci. USA* *114*, E3404–E3413.
- Labbadia, J., and Morimoto, R.I. (2015). The biology of proteostasis in aging and disease. *Annu. Rev. Biochem.* *84*, 435–464.
- Lang, A.B., John Peter, A.T.A.T., Walter, P., and Kornmann, B. (2015). ER-mitochondrial junctions can be bypassed by dominant mutations in the endosomal protein Vps13. *J. Cell Biol.* *210*, 883–890.
- Lee, S., Lim, W.A., and Thorn, K.S. (2013). Improved blue, green, and red fluorescent protein tagging vectors for *S. cerevisiae*. *PLoS ONE* *8*, e67902.
- Lesage, S., Drouet, V., Majounie, E., Deramecourt, V., Jacoupy, M., Nicolas, A., Cormier-Dequaire, F., Hassoun, S.M., Pujol, C., Ciura, S., et al.; French Parkinson's Disease Genetics Study (PDG); International Parkinson's Disease Genomics Consortium (IPDGC) (2016). Loss of VPS13C Function in Autosomal-Recessive Parkinsonism Causes Mitochondrial Dysfunction and Increases PINK1/Parkin-Dependent Mitophagy. *Am. J. Hum. Genet.* *98*, 500–513.
- Liu, C., Apodaca, J., Davis, L.E., and Rao, H. (2007). Proteasome inhibition in wild-type yeast *Saccharomyces cerevisiae* cells. *Biotechniques* *42*, 158–160, 162.
- Luo, W., Sun, W., Taldone, T., Rodina, A., and Chiosio, G. (2010). Heat shock protein 90 in neurodegenerative diseases. *Mol. Neurodegener.* *5*, 24.
- Malinowska, L., Kroschwald, S., Munder, M.C., Richter, D., and Alberti, S. (2012). Molecular chaperones and stress-inducible protein-sorting factors coordinate the spatiotemporal distribution of protein aggregates. *Mol. Biol. Cell* *23*, 3041–3056.
- McClellan, A.J., Scott, M.D., and Frydman, J. (2005). Folding and quality control of the VHL tumor suppressor proceed through distinct chaperone pathways. *Cell* *121*, 739–748.
- Medicherla, B., Kostova, Z., Schaefer, A., and Wolf, D.H. (2004). A genomic screen identifies Dsk2p and Rad23p as essential components of ER-associated degradation. *EMBO Rep.* *5*, 692–697.
- Miller, S.B., Ho, C.-T., Winkler, J., Khokhrina, M., Neuner, A., Mohamed, M.Y., Guilbride, D.L., Richter, K., Lisby, M., Schiebel, E., et al. (2015a). Compartment-specific aggregates direct distinct nuclear and cytoplasmic aggregate deposition. *EMBO J.* *34*, 778–797.
- Miller, S.B.M., Mogk, A., and Bukau, B. (2015b). Spatially organized aggregation of misfolded proteins as cellular stress defense strategy. *J. Mol. Biol.* *427*, 1564–1574.
- Ogrodnik, M., Salmonowicz, H., Brown, R., Turkowska, J., Średniawa, W., Patbiraman, S., Amen, T., Abraham, A.C., Eichler, N., Lyakhovetsky, R., and Kaganovich, D. (2014). Dynamic JUNQ inclusion bodies are asymmetrically inherited in mammalian cell lines through the asymmetric partitioning of vimentin. *Proc. Natl. Acad. Sci. USA* *111*, 8049–8054.
- Öling, D., Eisele, F., Kvint, K., and Nyström, T. (2014). Opposing roles of Ubp3-dependent deubiquitination regulate replicative life span and heat resistance. *EMBO J.* *33*, 747–761.
- Park, S.H., Bolender, N., Eisele, F., Kostova, Z., Takeuchi, J., Coffino, P., and Wolf, D.H. (2007). The cytoplasmic Hsp70 chaperone machinery subjects misfolded and endoplasmic reticulum import-incompetent proteins to degradation via the ubiquitin-proteasome system. *Mol. Biol. Cell* *18*, 153–165.
- Perez-Riverol, Y., Csordas, A., Bai, J., Bernal-Llinares, M., Hewapathirana, S., Kundu, D.J., Inuganti, A., Griss, J., Mayer, G., Eisenacher, M., et al. (2019). The PRIDE database and related tools and resources in 2019: improving support for quantification data. *Nucleic Acids Res.* *47* (D1), D442–D450.
- Prodromou, C. (2016). Mechanisms of Hsp90 regulation. *Biochem. J.* *473*, 2439–2452.
- Rampoldi, L., Dobson-Stone, C., Rubio, J.P., Danek, A., Chalmers, R.M., Wood, N.W., Verellen, C., Ferrer, X., Malandrini, A., Fabrizi, G.M., et al. (2001). A conserved sorting-associated protein is mutant in chorea-acanthocytosis. *Nat. Genet.* *28*, 119–120.
- Reynolds, E.S. (1963). The use of lead citrate at high pH as an electron-opaque stain in electron microscopy. *J. Cell Biol.* *17*, 208–212.
- Ritchie, M.E., Phipson, B., Wu, D., Hu, Y., Law, C.W., Shi, W., and Smyth, G.K. (2015). limma powers differential expression analyses for RNA-sequencing and microarray studies. *Nucleic Acids Res.* *43*, e47.
- Saarikangas, J., and Barral, Y. (2015). Protein aggregates are associated with replicative aging without compromising protein quality control. *eLife* *4*, e06197.
- Sahasrabudhe, P., Rohrberg, J., Biebl, M.M., Rutz, D.A., and Buchner, J. (2017). The Plasticity of the Hsp90 Co-chaperone System. *Mol. Cell* *67*, 947–961.e5.
- Schneider, Caroline, A, Rasband, Wayne, S, and Eliceiri, Kevin, W. (2012). NIH Image to ImageJ: 25 years of image analysis. *Nature Methods* *9*, 671–675. <https://doi.org/10.1038/nmeth.2089>.
- Seong, E., Insolera, R., Dulovic, M., Kamsteeg, E.J., Trinh, J., Brüggemann, N., Sandford, E., Li, S., Ozel, A.B., Li, J.Z., et al. (2018). Mutations in VPS13D lead to a new recessive ataxia with spasticity and mitochondrial defects. *Ann. Neurol.* *83*, 1075–1088.
- Shelton, L.B., Koren, J., 3rd, and Blair, L.J. (2017). Imbalances in the Hsp90 chaperone machinery: Implications for tauopathies. *Front. Neurosci.* *11*, 724.
- Sinclair, D.A., and Guarente, L. (1997). Extrachromosomal rDNA circles—a cause of aging in yeast. *Cell* *91*, 1033–1042.
- Smeal, T., Claus, J., Kennedy, B., Cole, F., and Guarente, L. (1996). Loss of transcriptional silencing causes sterility in old mother cells of *S. cerevisiae*. *Cell* *84*, 633–642.

- Sontag, E.M., Samant, R.S., and Frydman, J. (2017). Mechanisms and Functions of Spatial Protein Quality Control. *Annu. Rev. Biochem.* **86**, 97–122.
- Specht, S., Miller, S.B.M., Mogk, A., and Bukau, B. (2011). Hsp42 is required for sequestration of protein aggregates into deposition sites in *Saccharomyces cerevisiae*. *J. Cell Biol.* **195**, 617–629.
- Spiechowicz, M., Bernstein, H.G., Dobrowolny, H., Leśniak, W., Mawrin, C., Bogerts, B., Kuźnicki, J., and Filipiek, A. (2006). Density of Sgt1-immunopositive neurons is decreased in the cerebral cortex of Alzheimer's disease brain. *Neurochem. Int.* **49**, 487–493.
- Spokoini, R., Moldavski, O., Nahmias, Y., England, J.L., Schuldiner, M., and Kaganovich, D. (2012). Confinement to organelle-associated inclusion structures mediates asymmetric inheritance of aggregated protein in budding yeast. *Cell Rep.* **2**, 738–747.
- Taxis, C., Vogel, F., and Wolf, D.H. (2002). ER-golgi traffic is a prerequisite for efficient ER degradation. *Mol. Biol. Cell* **13**, 1806–1818.
- Taxis, C., Hitt, R., Park, S.H., Deak, P.M., Kostova, Z., and Wolf, D.H. (2003). Use of modular substrates demonstrates mechanistic diversity and reveals differences in chaperone requirement of ERAD. *J. Biol. Chem.* **278**, 35903–35913.
- Theodoraki, M.A., Nillegoda, N.B., Saini, J., and Caplan, A.J. (2012). A network of ubiquitin ligases is important for the dynamics of misfolded protein aggregates in yeast. *J. Biol. Chem.* **287**, 23911–23922.
- Tong, A.H.Y., and Boone, C. (2006). Synthetic genetic array analysis in *Saccharomyces cerevisiae*. *Methods Mol. Biol.* **313**, 171–192.
- Trotter, E.W., Berenfeld, L., Krause, S.A., Petsko, G.A., and Gray, J.V. (2001). Protein misfolding and temperature up-shift cause G1 arrest via a common mechanism dependent on heat shock factor in *Saccharomyces cerevisiae*. *Proc. Natl. Acad. Sci. USA* **98**, 7313–7318.
- Usaj, M., Tan, Y., Wang, W., VanderSluis, B., Zou, A., Myers, C.L., Costanzo, M., Andrews, B., and Boone, C. (2017). TheCellMap.org: A web-accessible database for visualizing and mining the global yeast genetic interaction network. *G3 (Bethesda)* **7**, 1539–1549.
- Wagih, O., Usaj, M., Baryshnikova, A., VanderSluis, B., Kuzmin, E., Costanzo, M., Myers, C.L., Andrews, B.J., Boone, C.M., and Parts, L. (2013). SGAtools: one-stop analysis and visualization of array-based genetic interaction screens. *Nucleic Acids Res.* **41**, W591–W596.
- Wakabayashi, K., Engelender, S., Yoshimoto, M., Tsuji, S., Ross, C.A., and Takahashi, H. (2000). Synphilin-1 is present in Lewy bodies in Parkinson's disease. *Ann. Neurol.* **47**, 521–523.
- Wolfe, K.J., Ren, H.Y., Trepte, P., and Cyr, D.M. (2013). The Hsp70/90 co-chaperone, Sti1, suppresses proteotoxicity by regulating spatial quality control of amyloid-like proteins. *Mol. Biol. Cell* **24**, 3588–3602.
- Zhao, L., Yang, Q., Zheng, J., Zhu, X., Hao, X., Song, J., Lebacqz, T., Franssens, V., Winderickx, J., Nystrom, T., and Liu, B. (2016). A genome-wide imaging-based screening to identify genes involved in synphilin-1 inclusion formation in *Saccharomyces cerevisiae*. *Sci. Rep.* **6**, 30134.

STAR★METHODS

KEY RESOURCES TABLE

REAGENT or RESOURCE	SOURCE	IDENTIFIER
<b>Antibodies</b>		
Mouse monoclonal anti-GFP	Roche	Roche Cat# 11814460001; RRID:AB_390913
Mouse monoclonal anti-myc	Sigma-Aldrich	Cat# M4439; RRID:AB_439694
Mouse monoclonal anti-Pgk1	Thermo Fisher Scientific	Cat# 459250; RRID:AB_2532235
Mouse monoclonal anti-HA	Abcam	Cat# ab130275; RRID:AB_11156884
Rabbit polyclonal anti-Hsc82	Abcam	Cat# 30920; RRID:AB_873576
Rabbit polyclonal anti-GFP	Abcam	Cat# ab6556; RRID:AB_305564
Goat anti-Mouse IRDye 800CW	LI-COR	Cat# P/N 925-32210; RRID: AB_621842
Goat anti-Rabbit 10 nm gold	Electron Microscopy Sciences	#25108
<b>Chemicals, peptides, and recombinant proteins</b>		
Cycloheximide	Sigma-Aldrich	01810
Geldanamycin	Cayman chemicals	13355
MG132	Enzo Life Sciences	BML-PI102-0005
cOmplete protease inhibitor cocktail	Roche	11697498001
Pefablock	Roche	11429868001
L-Azetidine-2-carboxylic acid (AZC)	Bachem	4019045
Wheat Germ Agglutinin Alexa Fluor 555 conjugate (WGA-orange)	Invitrogen	W32464
<b>Critical commercial assays</b>		
FuGENE HD Transfection Reagent	Promega	E2311
4-12% gradient 26 well Criterion XT Bis-Tris Protein gel	Bio-Rad	3450125
PVDF membrane	Millipore	IPFL00005
Odyssey Blocking buffer in PBS	LI-COR	927-40000
<b>Deposited data</b>		
Affinity-based mass spectrometry data for interactors of Sgt1 at 30°C and 42°C	This paper (Table S2) and ProteomeXchange	PXD016174
<b>Experimental models: Cell lines</b>		
Human: HeLa	ATCC (Manassas, VA)	ATCC Cat# CCL-2, RRID:CVCL_0030
<b>Experimental models: Organisms/Strains</b>		
<i>S. cerevisiae</i> strain Y7092 SGA query: Strain background: S288C MAT $\alpha$ ( <i>can1<math>\Delta</math>::STE2pr-Sp_his5 lyp1<math>\Delta</math> his3<math>\Delta</math>1 leu2<math>\Delta</math>0 ura3<math>\Delta</math>0 met15<math>\Delta</math>0</i> )	Boone laboratory	N/A
<i>S. cerevisiae</i> strain BY4741: Strain background: S288C genotype: MAT $\alpha$ <i>his3<math>\Delta</math>1 leu2<math>\Delta</math>0 met15<math>\Delta</math>0 ura3<math>\Delta</math>0</i>	EUROSCARF	Y00000
All <i>Saccharomyces cerevisiae</i> yeast strains used in this study were of the S288C or BY4741 background and are listed in Table S3	EUROSCARF or Nyström laboratory	N/A
<b>Oligonucleotides</b>		
VHL FWD: ATTGTTTCTTTTCTACTCAACTTAAAGTATACATACGCTGCATG Catgccccggaggcggaactgg	this paper	N/A

(Continued on next page)

**Continued**

REAGENT or RESOURCE	SOURCE	IDENTIFIER
VHL REV GTCACCTGGCAAACGACGATCTTCTTAGGGGCAGAGTTAACCATatctcccatccgttgatgtgc	this paper	N/A
HygExURA3 up: CTTAACCCAACTGCACAGAACAAAACCTGCAGGAAACGAAGATAAATCatgggtaaaaagcctgaactcac	this paper	N/A
HygExURA3 down CTAATTTGTGAGTTTAGTATACATGCATTTACTTATAATACAGTTTTtattcctttgccctcgagc	this paper	N/A
HUL5 S1 GCGTTATAATTTATCTCAAGCAGCATTTCAAAGGATTCTGACTTAAAATGcgtacgctgcaggtcgac	this paper	N/A
HUL5 S4 GTCCTATTCCTAAATTGACATTTCTTCTCCTTGTTTGACCGGTGAAGTTTAAcatcgatgaattctctgtcg	this paper	N/A
SGT1 S1 GTCTTTTAAAGGTTAAAGAGGTAGTTGTTTTAAAGGAAACGAAAAGAAAATGcgtacgctgcaggtcgac	this paper	N/A
SGT1 S4 CTCATCATACAAAGCTTTGTAGGCAGTTTTTAAATCTTTTTCAACAGGcatcgatgaattctctgtcg	this paper	N/A
Hsp82 S3 TGAAGAGGTTCCAGCTGACACCGAAATGGAAGAGGTAATGcgtacgctgcaggtcgac	this paper	N/A
Hsp82 S2 TTTTGTATAACCTATTCAAGGCCATGATGTTCTACCTAatcgatgaattcgagctcg	this paper	N/A

**Recombinant DNA**

SGT1A/ SUGT1A 333 AA short version from 1 to 1002, CAC51433_1 from 1 to 1002_40bps overlap CATGGACGAGCTGTACAAGTCCGGACTCAGATCTCGAGCTcAtAGGCGGGCGCTGCAGCAGGAACGCAACATCCCAGAGGTTTTCAGAGCTTCTCGGATGCCCTAATCGACGAGGACCCCCAGGCGCGTTAGAGGAGCTGACTAAGGCTTTGGAACAGAAACCAGATGATGCACAGTATTATTGTCAAAGAGCTTATTGTCACATTTCTTTGGGAATTA CTGTGTTGCTGTTGCTGATGCAAAGAAGTCTCTAGAACTCAATCCAAA TAATCCACTGCTATGCTGAGAAAAGGAATATGTGAATACCATGAAAA AACTATGCTGCTGCCCTAGAACTTTTACAGAAGGACAAAAATTAG ATAGTGCAGATGCTAATTTTCAGTGTCTGGATTAAGGTGTCAAGAAG CTCAGAATGGCTCAGAATCTGAGGTGTGGACTCATCAGTCAAAAATC AAGTATGACTG GTATCAAACAGAATCTCAAGTAGTCATTACACTTATG ATCAAGAATGTTTCAAGAAGATGATGTAATGTGGAATTTTCAGAAAA GAGTTGTCTGCTTTTGGTTAAACTTCTCTGGAGAGGATTACAATTTG AAAGTGGAACTTCTTATCCTATAATACCAGAACAGAGCACGTTTAAAGTACTTTCAACAAGATTGAAATTAAGTGAAGGCAAGGCTGTG AGATGGGAAAAGCTAGAGGGGCAAGGAGATGTGCCTACGCCAAAAC AATTCGTAGCAGATGTAAGAACCTATATCCATCATCTCCTTATAC AAGAAATTTGGATAAATTTGTTGGTGTGAGATCAAAGAAGAAGAAAAGA ATGAAAAGTTGGAGGGAGATGCAGCTTTAAACAGATTATTTTCAGCAGA TCTATTCAGATGGTTCTGATGAAGTGAACGTGCCATGAACAAATCCT TTATGGAGTCGGGTGGTACAGTTTTGAGTACCAACTGGTCTGATGTAG GTAAAAGGAAAGTTGAAATCAATCCTCCTGATGATGGAATGAAAAA AGTACTAAGGGCCCCGGATCCACCGGATCTAGATAACTGATCATAATC	gBlocks from IDT	N/A
---	------------------	-----

All plasmids used in this study are listed in [Table S4](#)

This study

N/A

**Software and algorithms**

ImageJ	(Schneider et al., 2012)	<a href="https://imagej.nih.gov/ij/">https://imagej.nih.gov/ij/</a>
TheCellMap	(Usaj et al., 2017)	<a href="https://thecellmap.org">https://thecellmap.org</a>

**Other**

Zeiss Axio Observer .Z1 inverted microscope with Apotome and AxioCam 506 camera	Carl Zeiss	N/A
LI-COR Odyssey Infrared scanner	LI-COR	N/A
Criterion Cell	Bio-Rad	1656001
Wet blotting system (Criterion Blotter)	Bio-Rad	1704070

## RESOURCE AVAILABILITY

### Lead contact

Further information and requests for reagents may be directed to, and will be fulfilled by the Lead Contact, Thomas Nyström, ([thomas.nystrom@cmb.gu.se](mailto:thomas.nystrom@cmb.gu.se)).

### Materials availability

All unique reagents generated in this study are available from the Lead Contact without restriction.

### Data and code availability

All datasets generated or analyzed during this study are included in the article, except for microscopy images used for quantitative analysis, which are available upon request. Affinity based mass spectrometry data are also deposited at ProteomeXchange with the accession code: PXD016174.

## EXPERIMENTAL MODEL AND SUBJECT DETAILS

### Yeast strains

Strains and plasmids are listed in [Tables S3](#) and [S4](#), respectively. The strains used in this study are derivatives of BY4741 ([Brachmann et al., 1998](#)) or haploid strains generated with the SGA methodology ([Tong and Boone, 2006](#)) (SGA library). Overexpression, N-terminal GFP tagged strains and additional deletions were generated via homologous recombination with the molecular toolbox ([Janke et al., 2004](#)). The mRuby2 tag was amplified from plasmid pFA6a-link-yomRuby2-Kan ([Lee et al., 2013](#)) via PCR with S2 and S3 primers specific for *HSP82* and recombined into the C- terminus of genomic *Hsp82*. Overexpression of the *SGT1* and *HUL5* open reading frames was achieved by integration of the *GPD* promoter amplified from pYM-N15 with primers S1 and S4, specific to *SGT1* or *HUL5*, respectively. *GPD* promoter and N-terminal EGFP tagging of *SGT1* was achieved by amplification from pYM-N17 with primers *SGT1* S1 and S4. Cells were selected on YPD clonNat plates and correct integration was verified by PCR. Primer sequences can be found in the [Key Resources Table](#).

Cells were cultured at 30°C, or at 22°C in case of temperature sensitive strains, in either rich YPD medium, in complete synthetic medium (CSM) or in synthetic dropout (SD) media lacking the appropriate components ([Amberg et al., 2005](#)).

### Mammalian cell culture

HeLa cells were grown in DMEM media (with 4500 mg/L glucose, 25 mM HEPES, MERCK) supplemented with 10% FCS, 2 mM glutamine, 100 U/ml penicillin, and 100 µg/ml streptomycin (Invitrogen) at 37°C in a humidified atmosphere of 5% CO<sub>2</sub>.

## METHOD DETAILS

### Plasmid constructions

Plasmid pFE30 expressing VHL-Leu2 was constructed by homologous recombination into plasmid pFE15 ([Eisele and Wolf, 2008](#)) expressing  $\Delta$ ssCL\*. Therefore, the sequence encoding VHL was amplified by PCR from vector pESC-LEU-GFP-VHL with primers VHL Fwd and VHL Rev. Purified PCR product was co-transformed into yeast cells with Bsu36I digested vector pFE15 and selected for growth on SD-Ura plates. The resulting plasmid pFE30 was rescued and tested by sequencing.

For replacing the *URA3* selection marker in plasmid pFE15 and pFE30, the *hphNT1* cassette from pFA6a-hphNT1 ([Janke et al., 2004](#)) was amplified with primers HygExURA3 up and HygExURA3 down. Purified PCR product was transformed into yeast cells harboring vector pFE15 or pFE30 and selected for growth on YPD hygromycin B plates. Resulting plasmids pFE35 and pFE36 were rescued and tested by sequencing. For construction of *phSgt1* expressing human Sgt1 with a N-terminal EGFP tag for expression in animal cell lines SUGT1/SGT1A coding double stranded DNA was synthesized flanked with 40 bps overhangs compatible to the multiple cloning site of pEGFP-C1. SGT1A coding DNA and vector were digested with *Apal* and *SacI*, ligated and transformed into DH5 $\alpha$  cells. The resulting plasmid *phSgt1* (pFE67) was tested by sequencing. Please see [Key Resources Table](#) for oligonucleotide and sequence details, [Table S4](#) for plasmid details.

### Genome-wide screen for stabilizers of two misfolding proteins

The yeast strains used (S228C background) were grown in synthetic drop-out media with corresponding antibiotics. SGA mating of query strains (Y7092) containing  $\Delta$ ssCL\* (pFE15) or VHL-Leu2 (pFE30) into the yeast deletion collection SGAV2 array and a conditional temperature sensitive (ts) allele collection (TSV5 array) (both layouts from the Boones laboratory, spotted in a 1536-spot format by using a SINGER ROTOR HDA Robot (Singer Instrument Co. Ltd.)) were performed as previously described in [Tong and Boone \(2006\)](#). Selected haploid crossed cells were spotted on SD/MSG-His/Arg/Lys/Ura/+canavanine/thialysine/G418 and SD/MSG-His/Arg/Lys/Ura/Leu/+canavanine/thialysine/G418. Images were taken after two days growth at 30°C and colony sizes were analyzed as previously described ([Costanzo et al., 2010](#); [Wagih et al., 2013](#)).

Mutants displaying good growth with a score of 1 or higher are indicated in [Table S1](#). Common hits from  $\Delta$ ssCL\* and VHL-Leu2 screen were used for analysis with the [TheCellMap.org](http://TheCellMap.org).

### Spot tests

For  $\Delta$ ssCL\*, CTL\*, Leu2-myc spot tests overnight pre-cultured cells expressing  $\Delta$ ssCL\*, CTL\* or Leu2-myc were diluted to an OD of  $A_{600} = 0.5$  and spotted in a 5-fold dilution series on SD-Ura and SD-Ura-Leu media. Plates were incubated at 30°C for 3–4 days.

For complementation assays strains were cotransformed with a plasmid expressing  $\Delta$ ssCL\* or VHL-Leu2 with a *hphNT1* selection marker (pFE35 or pFE36, respectively) and with MoBY plasmids expressing wild-type alleles of the corresponding mutant strains, or the empty vector control (p5586) ([Ho et al., 2009](#)). 5-fold dilutions of cells were spotted on SD-Ura +hygromycin B and SD-Ura-Leu +hygromycin B. For complementation of the *sgt1-3* allele by the GFP-SGT1 fusion allele, strains were crossed to obtain heterozygote diploid strains and tested by spot test like described below.

For heat sensitivity assays exponentially growing cells were diluted to  $OD_{600} = 0.5$  and then spotted on YPD plates, in a tenfold dilution series. Plates were incubated at the indicated temperatures for 2–3 days prior to imaging.

### Co-immuno purifications (Co-IP)

Cells were inoculated and grown over night in complete synthetic media (CSM), SD-Ura (if carrying pFE15 plasmid) or SD-His (pEGFP ctrl plasmid) to  $OD_{600} = 0.7$ -0.8. Fifty  $OD_{600}$  of exponentially grown cells were harvested and washed twice with ice-cold water (2 min at 3220xg, 4°C). Cells were washed once with ice-cold IP buffer (115 mM KCl, 5 mM NaCl, 2 mM  $MgCl_2$ , 1 mM EDTA/NaOH pH 8.0, 20 mM HEPES/KOH pH 7.45) and resuspended in a final volume of 300  $\mu$ l IP buffer. Cells were snap frozen and kept at  $-80^\circ\text{C}$ . A volume of 200  $\mu$ l glass beads, 1 mM DTT, 0.5  $\mu$ g/ml Pefabloc SC, 1x cComplete (Roche) were added (calculated for 1 mL final volume) and cells were opened by 10 times vortexing for 45 s with 1 min chilling on ice between the cycles. Lysates were transferred to a new tube and buffer was added to 1 mL final volume. Lysates were incubated with 0.5% Nonidet P-40 (Roche) for 20 min on ice, followed by centrifugation at 16000xg for 20 min at 4°C. 800  $\mu$ l of pre-cleared cell lysate was incubated with 20  $\mu$ l bed volume GFP-TrapA beads (Chromotek) to pull down GFP tagged proteins for 1 h at 4°C on an over-head rotator. Beads were pelleted by centrifugation at 8000 rpm and washed 4 times with IP buffer containing 0.5% Nonidet P-40. For co-IP experiments with Hsp90 inhibition, 50  $\mu$ M geldanamycin (GA) was added to cells 30 min prior of harvest and kept at this concentration during lysis, co-IP and washing. For immunoblot analysis beads were boiled for 5 min at 95°C in 2x loading buffer/5% beta-mercaptoethanol. For mass spectrometry analysis beads were subjected for a final wash in 50 mM TEAB buffer followed by 2 sequential rounds of elution in 1% formic acid. Elutions were pooled and subsequently treated as described below in section sample preparation and TMT labeling.

### In vivo ubiquitination assay

Samples were principally prepared like described in [Geng and Tansey \(2008\)](#). Cells harboring plasmids expressing His6-Ub and  $\Delta$ ssCL\* or empty control vector were grown in SD-Ura hygromycin B media to early exponential growth phase. His6-Ub expression was induced by addition of 0.1 mM  $CuSO_4$  4 h previous to harvest. 100  $OD_{600}$  of cells were harvested (4 min at 3220xg, 4°C) and washed with ice cold  $dH_2O$ . 1% of the cells were used as expression level control and were lysed as described below in section western blotting. Cells were lysed with a MP FastPrep (level 5.5, 30 s, 5 min on ice, 4 cycles) in 800  $\mu$ l lysis buffer (6 M Guanidine-HCl, 100 mM  $Na_2HPO_4/NaH_2PO_4$  at pH 8, 10 mM Imidazole, 250 mM NaCl, 0.5% (v/v) NP-40 (Roche) and 300  $\mu$ l glass beads. Lysates were cleared by centrifugation at 16000xg for 10 min. Supernatant was incubated for 2 h in cold room on rotary wheel with Ni-NTA agarose beads to capture ubiquitinated proteins. Beads were spun down (2500xg, 1 min) and washed two times with lysis buffer and three times with wash buffer (50 mM  $Na_2HPO_4/NaH_2PO_4$  at pH 8, 250 mM NaCl, 20 mM Imidazole, 0.5% (v/v) NP-40. Agarose resin was incubated for 10 min at 70°C in 100  $\mu$ l urea loading buffer (see western blotting section). Proteins were separated by SDS-PAGE and detected using anti-myc specific antibodies.

### Cycloheximide chase

Exponentially growing cells expressing  $\Delta$ ssCL\*, CTL\*, CTG\* or CPY\*HA were harvested and resuspended in synthetic drop out media. GFP-Sgt1-3 expressing cells were resuspended in YPD media. 50  $\mu$ M geldanamycin (GA) was added to growing cells 30 min prior of chase where indicated. Protein expression was shut off by addition of cycloheximide (1.77 mM final). 2  $OD_{600}$  of cells were harvested by adding to ice cold  $NaN_3$  (30 mM final concentration) at indicated time-points. Protein samples for western blotting were prepared as described below.

### Metabolic chase

Cells expressing VHL-GFP were grown in SD-Leu containing 2% (w/v) galactose. For shut-off of VHL-GFP expressing cells were shifted in exponential growth phase to SD-Leu containing 2% glucose. 2  $OD_{600}$  of cells were harvested at indicated time points by adding to ice cold  $NaN_3$  (30 mM final concentration). Protein samples for western blotting were prepared as described below.

### Western blotting

Samples were principally prepared as described in [Hwang et al. \(2009\)](#). Cells were resuspended in 1 mL of ice cold 0.2 M NaOH and incubated for 20 min on ice. Cells were pelleted and resuspended in 100  $\mu$ l urea loading buffer (8 M urea in 1x loading buffer; 50 mM

Tris/HCl pH 6.8, 2.5 mM EDTA/NaOH pH 8.0, 2% (w/v) Na-Dodecylsulfat (SDS), 0.05% (w/v) bromphenol blue). Prior to use 1% (v/v) beta-mercaptoethanol and complete protease inhibitor (Roche) was added to urea loading buffer. After incubation for 10 min at 70°C, samples were centrifuged at 13000xg for 1 min. 15 µl were loaded on a 4%–12% gradient 26 well Criterion XT Bis-Tris Protein gel (Bio-Rad). Gels were transferred on PVDF membrane (Millipore) with a wet blotting system (Criterion Blotter, Bio-Rad). The blots were incubated in Odyssey blocking buffer (LI-COR) for 1 h at room temperature prior to probing with primary antibodies in PBS-T. Membranes were washed and incubated with the appropriate secondary antibody (LI-COR, IRdye secondary antibodies). Membranes were scanned on a LI-COR Odyssey scanner, and western blots were quantified using ImageJ (NIH). Please see [Key Resources Table](#) for antibodies, reagents, and equipment details.

### Replicative lifespan assay

Exponentially growing cells were plated on YPD plates and allowed to recover before assayed for replicative lifespan. A micromanipulator (MSM 400, Singer instruments) was used to select mother cells and to remove their daughters for assessing of replicative age.

### Isolation of old mother cells

Old cells expressing Hsp104-GFP were isolated using the magnetabind biotin-streptavidin system according to established protocols (Hill et al., 2016; Sinclair and Guarente, 1997; Smeal et al., 1996). Biotin labeled cells were isolated after culturing for one day. The median age of the old cells was determined by counting of bud scars after formaldehyde fixation and staining cells with 10 µg/mL Wheat Germ Agglutinin Alexa Fluor® 555 conjugate (WGA, Life Technologies).

### Assessment of colony forming units (CFU)

Cells were grown in CSM to mid-exponential phase at 30°C. Cells were shifted to 42°C for 30 min, and then allowed to recover at 30°C for 90 min. Control cells were kept growing at 30°C during that period and then adjusted to same optical density. Cells were diluted sequentially one to hundred, followed by a two or ten-fold dilution. 100 µl cell suspension were plated on CSM agar plates and number of CFU assessed after growth for 5 days at 22°C.

### Hsp104, Hsp42 and Guk1-7 protein aggregation induction

Fluorescent protein tagged cells were grown to mid-exponential phase at 30°C in CSM and then shifted to 38°C, or to 42°C for 30 min and then back to 30°C. Samples were taken at indicated time points, fixed with formaldehyde (3.7% final concentration) for 30 min, washed three times with PBS and observed by fluorescence microscopy (see below).

### Sgt1, Hsp82, Vps13, Hsp42-, and synphilin-1 foci formation assay

Fluorescent protein tagged cells were grown in CSM (or SD-Ura in case of dsRed-synphilin-1) to mid-exponential phase at 30°C. If cells were to be treated with 26S proteasome inhibitor MG132 (75 µM final concentration, EnzoLifesciences), SDS was added to growing cells to a final concentration of 0.003% three hours prior to addition of the drug and heat shock (Liu et al., 2007). Geldanamycin (GA) was added to a final concentration of 70 µM prior to heat shock (Theodoraki et al., 2012). For induction of Hsp104 or Vps13 and synphilin-1 foci, cells were shifted to 42°C water bath for 30 min. Then cells were briefly spun at 5000xg and observed with a Zeiss Axio Observer Z1 inverted fluorescence microscope, using Plan Apo 100X oil objective NA:1.4 and the following filter sets: 38 HEeGFP, 45 HQ TexasRed.

### Cell culture and transient transfection

HeLa cells were grown on glass coverslips in DMEM (with 4500 mg/L glucose, 25 mM HEPES, MERCK) supplemented with 10% FCS, 2 mM glutamine, 100U/ml penicillin, and 100 µg/ml streptomycin (Invitrogen) at 37°C in a humidified atmosphere of 5% CO<sub>2</sub>. Cells were transiently transfected with eGFP-C1-SUGT1 or eGFP-C1-EV by using FuGENE HD (Promega). 18–22 h post-transfection cells were treated with MG132 (5 µM) or geldanamycin (75 µM) or DMSO as a control for 1 h (Ogrodnik et al., 2014). Cells were heat shocked at 40°C for 15 min and directly observed under the microscope (see above).

### Electron microscopy

#### High pressure freezing and freeze substitution of yeast cells

Exponentially growing GFP-Sgt1 expressing yeast cells were grown at 30°C or shifted to 42°C for 30 min prior to harvesting by filtering and high pressure freezing in a Wohlwend Compact 03 (M. Wohlwend GmbH, Sennwald, Switzerland). Freeze substitution was carried out in a Leica EM AFS2 (Leica Microsystems, Vienna, Austria) using 2% uranyl acetate dissolved in 10% methanol and 90% acetone for 1 h at –90°C (Höög et al., 2014). The temperature was raised to –50°C, 2.9°C per hour, during two washes in acetone. The cells were infiltrated with Lowicryl HM20 (Polysciences, Warrington, PA) mixed with acetone (1:4, 2:3, 1:1, 4:1) and three times with pure Lowicryl, each step lasting 2 hours. The resin was polymerized with UV light 72 h at –50°C followed by 24 hr at room temperature. 70 nm ultra-thin sections were produced using a Reichert-Jung Ultracut E Ultramicrotome (C. Reichert, Vienna, Austria) and an ultra 45° diamond knife (Diatome, Biel, Switzerland). The thin sections were placed on copper grids coated with 1% Formvar and on-section contrast stained. Micrographs were taken on a Tecnai T12 electron microscope equipped with a Ceta CMOS 16M camera (FEI Co., Eindhoven, the Netherlands) operated at 120 kV.

### Immunoelectron microscopy

Grids were fixed in 1% paraformaldehyde in PBS for 10 min at room temperature, washed 3 × 1 min in PBS, and blocked for 1 h in 0.8% BSA + 0.1% fish skin gelatin in PBS at room temperature. For detection of GFP-Sgt1, grids were incubated in a 1 to 30 dilution of rabbit anti-GFP (ab6556, abcam, Cambridge, UK) at 4°C over-night followed by a 1 to 20 dilution of goat anti-rabbit 10 nm gold (#25108, Electron Microscopy Sciences, Hatfield, PA) for 1 h at room temperature. 3 × 20 min wash steps were carried out in PBS after incubations with each antibody. Antibodies were fixed in 1% glutaraldehyde in dH<sub>2</sub>O for 1 h and washed 3 × 1 min in dH<sub>2</sub>O. 2% uranyl acetate and Reynold's lead citrate were used for on-section contrast staining (Reynolds, 1963). Imaging as above.

### Mass spectrometry

#### Sample preparation and TMT labeling

Cysteines were reduced with dithiothreitol (Biomol) at 56°C for 30 min (10 mM in 50 mM HEPES (Biomol), pH 8.5), and further alkylated with iodoacetamide (Merck) at room temperature, in the dark for 30 min (20 mM in 50 mM HEPES, pH 8.5). For sample clean up and digestion, the SP3 protocol (Hughes et al., 2014) was used and trypsin (sequencing grade, Promega) was added (enzyme to protein ratio 1:20) for overnight digestion at 37°C. Next day, peptides were extracted and labeled with TMT10plex Isobaric Label Reagent (ThermoFisher) according to the manufacturer's instructions. For further sample clean up an OASIS® HLB μElution Plate (Waters) was used. Offline high pH reverse phase fractionation was carried out on an Agilent 1200 Infinity high-performance liquid chromatography system, equipped with a Gemini C18 column (3 μm, 110 Å, 100 × 1.0 mm, Phenomenex).

#### Mass spectrometry data acquisition

An UltiMate 3000 RSLC nano LC system (Dionex) fitted with a trapping cartridge (μ-Precolumn C18 PepMap 100, 5 μm, 300 μm i.d. × 5 mm, 100 Å, Thermo Fisher) and an analytical column (Acclaim PepMap 100, 75 μm × 50 cm, nanoViper column, Thermo Fisher). Trapping was carried out with a constant flow of solvent A (0.1% formic acid in water) at 30 μL/min onto the trapping column for 6 min. Subsequently, peptides were eluted via the analytical column with a constant flow of 0.3 μL/min with increasing percentage of solvent B (0.1% formic acid in acetonitrile) from 2% to 4% in 4 min, from 4% to 8% in 2 min, then 8% to 28% for a further 96 min, and finally from 28% to 40% in another 10 min. The outlet of the analytical column was coupled directly to a QExactive plus (Thermo Fisher) mass spectrometer using the proxeon nanoflow source in positive ion mode.

The peptides were introduced into the QExactive plus via a Pico-Tip Emitter 360 μm OD × 20 μm ID; 10 μm tip (New Objective) and an applied spray voltage of 2.3 kV. The capillary temperature was set at 320°C. Full mass scan was acquired with mass range 375–1200 m/z in profile mode in the FT with resolution of 70000. The filling time was set at maximum of 250 ms with a limitation of 3 × 10<sup>6</sup> ions. Data dependent acquisition (DDA) was performed with the resolution of the Orbitrap set to 35000, with a fill time of 120 ms and a limitation of 2 × 10<sup>5</sup> ions. A normalized collision energy of 32 was applied. A loop count of 10 with count 1 was used and a minimum AGC trigger of 2e<sup>2</sup> was set. Dynamic exclusion time of 30 s was used. The peptide match algorithm was set to 'preferred' and charge exclusion 'unassigned', charge states 1, 5 - 8 were excluded. MS<sup>2</sup> data was acquired in profile mode.

#### MS data analysis

IsobarQuant (Franken et al., 2015) and Mascot (v2.2.07) were used to process the acquired data, which was searched against a UniProt *Saccharomyces cerevisiae* proteome database (UP000002311) containing common contaminants and reversed sequences. The following modifications were included into the search parameters: Carbamidomethyl (C) and TMT10 (K) (fixed modification), Acetyl (N-term), Oxidation (M) and TMT10 (N-term) (variable modifications). For the full scan (MS1) a mass error tolerance of 10 ppm and for MS/MS (MS2) spectra of 0.02 Da was set. Further parameters were set: Trypsin as protease with an allowance of maximum two missed cleavages: a minimum peptide length of seven amino acids; at least two unique peptides were required for a protein identification. The false discovery rate on peptide and protein level was set to 0.01. The protein output files of IsobarQuant were processed using the R programming language (<https://www.r-project.org>). As a quality filter, only proteins that were quantified with at least 2 unique peptides were used for the downstream analysis. Raw TMT reporter ion signals (signal\_sum columns) were first batch-cleaned using the removeBatchEffect function from the limma package (Ritchie et al., 2015) and further normalized using the vsn package (variance stabilization normalization; Huber et al., 2002). Missing values were imputed using the knn option of the impute function using the Msnbase package (Gatto and Lilley, 2012). Proteins were tested for differential expression using limma again and called hits with a false discovery smaller 1% and a fold-change cut-off of 100%. The mass spectrometry proteomics data have been deposited to the ProteomeXchange Consortium via the PRIDE (Perez-Riverol et al., 2019) partner repository with the dataset identifier PXD016174 (See also [Key Resources Table](#)).

## QUANTIFICATION AND STATISTICAL ANALYSIS

To identify network regions significantly enriched for ΔssCL\* and VHL-Leu2 stabilization, as well as for physical interaction with Sgt1 at 30°C and 42°C, hits were analyzed with the help of [TheCellMap.org](#).

Lifespan assays were done in at least two replicates. Statistical analysis was performed using Logrank (Mantel-Cox test) in GraphPad Prism® 8.2.1 (Figures 2E, 2F, and S2F). Statistical analysis of Sgt1 localization by immunoelectron microscopy performed using Wilcoxon matched-pairs signed rank test in GraphPad Prism® 8.2.1 (Figure 3H).

All data in the bar graphs are presented as an average of n ≥ 3 replicates ± SEM. In figures, asterisks denote statistical significance as calculated by Student's t test \*p < 0.05, \*\*p < 0.005, \*\*\*p < 0.0005, unpaired two tailed t test using MS Excel.